ABSTRACT

DETERMINATION OF PHASE COMPOSITION OF SPUTTERED TANTALUM ON STEEL SUBSTRATES BY RESISTIVITY MEASUREMNETS

by
Younes Abbassi

The objective of this thesis was to develop a method of distinguishing between alpha and beta phases of tantalum films on steel substrates, using the four-point probe resistivity measurements. While there is a large difference between resistivities of the two Ta phases, the problem is challenging because the measurements are influenced by the low resistivity of steel.

For reference, the resistivity measurements of tantalum coatings (1-20 μm) on silicon and silicon dioxide substrates were conducted first. The measured resistivities were related to the crystallographic phase composition of Ta, which has lower resistivity in bcc form, α-phase, (13.5 to 42 μΩ.cm), than in the tetragonal form, β-phase, (87 to 157 μΩ.cm). The phase composition of Ta coatings was determined by X-ray diffraction (XRD) measurements, and the ratios of intensities of α-Ta (110) and β-Ta (002) peaks in XRD spectra were correlated with the measured resistivity values. Resistivities of the films deposited on silicon and silicon dioxide substrates were found to be same within the measurement error. The four-point probe measurements on these substrates were effective in distinguishing between films dominated by either α-Ta or β-Ta phase.

For thin Ta coatings on steel substrates the resistivity measurements are compromised by the "short circuit" effect of the steel, which has low resistivity, comparable to that of

the α-Ta phase. The effect of the substrate, which depends on the ratio of the probe spacing to the film thickness, was investigated for thick Ta coatings on steel (up to 0.8 mm), where the shorting effect was negligible, and different probe spacing (0.25 mm to 4 mm). The results are in agreement with the theoretical study of Weller, who found that resistivity measurements on conductive substrates are possible for a film thickness to probe spacing ratio equal or larger than 0.2 [14]. Microscopic four-point probes are suggested for thin films resistivity measurements. The development of microprobes with spacing as small as 500 nm has been recently reported. They will allow measuring the resistivity of films as thin as 2.5 μm on conducting substrates.

Ta coatings investigated in this work were deposited by DC magnetron sputtering. The surface of steel substrates was prepared using different methods, which included grinding, polishing, electrochemical cleaning and in-situ sputter etching. The substrate surface morphology and roughness was measured with atomic force microscopy (AFM). The smoothes steel surface was obtained by polishing with a suspension of 50 nm silica particles, which resulted in the surface roughness as low as 5.1 nm was measured on 30 μm x 30 μm scan area. Sputter etching in Ar gas resulted in the formation of characteristic cones on steel surface. No influence of various surface preparation methods on the phase of Ta was observed. However, cleaning, especially sputter-etching, was found to enhance film adhesion.

DETERMINATION OF PHASE COMPOSITION OF SPUTTERED TANTALUM ON STEEL SUBSTRATES BY RESISTIVITY MEASUREMNETS

by

Younes Abbassi

A Thesis
Submitted to the Faculty of
New Jersey Institute of Technology
In Partial Fulfillment of the Requirement for the Degree of
Masters in Electrical Engineering

Department of Electrical and Computer Engineering

May 2002

APPROVAL PAGE

DETERMINATION OF PHASE COMPOSITION OF SPUTTERED TANTALUM ON STEEL SUBSTRATES BY RESISTIVITY MEASUREMNETS

Younes Abbassi

Dr. Marek Sosnowski, Thesis Advisor — Date
Associate Professor of Electrical and Computer Engineering, NJIT.

Dr. Durga Misra, Committee Member — Date
Associate Professor of Electrical and Computer Engineering, NJIT.

Dr. Roy Cornely, Committee Member — Date
Professor of Electrical and Computer Engineering, NJIT.

BIOGRAPHICAL SKETCH

Author: Younes Abbassi

Degree: Masters of Science

Date: May 2002

Undergraduate and Graduate Education:

- Masters of Science in Electrical Engineering,
  New Jersey Institute of Technology, Newark, NJ, 2002

- Bachelor of Science in Electrical Engineering,
  New Jersey Institute of Technology, Newark, NJ, 2000

- Diplome D'etude Collegiale (DEC)
  Institut Teccart Inc, Montreal, Canada, 1995

Major: Electrical Engineering

To my beloved family
and
those individuals who have steadfastly supported me.

ACKNOWLEDGMENT

I want to deeply thank Dr. Marek Sosnowski for being my advisor for both my undergraduate senior project and my graduate thesis. By allowing me to work in the Ion Beam and Thin Film laboratory while working toward a master's degree in electrical engineering, I was able to acquire valuable knowledge and skills related to vacuum technology, especially thin film science. I felt very fortunate to be able to apply many of the engineering concepts that I have studied into real, practical situations while working in his laboratory. As a research supervisor, Dr. Marek Sosnowski provided me with invaluable resources, insights and intuition. He was also a constant source of support, encouragement, and reassurance during my work.

Special thanks are also given to Dr. Durgamadhab Misra for permitting me to use his Device Characterization Laboratory to conduct many of the essential experiments presented in this work. I also wish to express my gratitude to Professor Dr. Roy Cornely for reviewing the manuscript of this thesis and for constantly supporting and advising me.

Acknowledgements are made to Dr. Leszek Gladczuk for being my co-advisor. My fellow graduate students, Anamika Patel, Cheng Li, Sung Ming, and Sharanjeet Singh, are also deserving of recognition for their tremendous support and contributions to this work, without which it could not have been accomplished.

This research was funded in part by a grant from the U.S. Army.

TABLE OF CONTENTS

TABLE OF CONTENTS
(Continued)

Chapter **Page**

LIST OF TABLES

LIST OF FIGURES

LIST OF FIGURES
(Continued)

CHAPTER 1

INTRODUCTION

The objective of this thesis was to develop a method of distinguishing between alpha and beta phases of tantalum films on steel substrates, using the four-point probe resistivity measurements. While there is a large difference between resistivities of the two Ta phases, the problem is challenging because the measurements are influenced by the low resistivity of steel.

Currently, US Army gun barrels are coated with chromium in order to increase their service life by making them resistant to erosive and corrosive wear. However, the major drawback of hard chrome plating is that it results in environmental and health exposure problems due to the use of hexavalent chromium. In addition, the next–generation US Army guns must meet demands for higher performance and accurate delivery of projectiles which use higher energy propellants in a higher temperature corrosive environment. Therefore, sputtering of a refractory material such as tantalum can produce a superior substitute for chromium plating at a lower cost and lower environmental impact. In the following pages, some background information is provided on sputtering deposition and it's important applications. Explanations as to why tantalum, especially in its alpha form, has been promoted as a good candidate for a gun barrel coating is also given.

Tantalum films have many important applications in a variety of fields, including electronics, X-ray optics, and chemical apparatus. They offer many attractive properties such as high melting point, good thermal conductivity, high resistance to corrosive and erosive wear, high ductility and durability [1]. Its chemical stability and robust mechanical properties make it a very desirable material for electronic components fabrication, such as thin film capacitors and resistors. In copper metalization, tantalum and tantalum nitrites are used as an effective diffusion barrier in ULSI of Si integrated circuits. Recently, the IC industry is shifting from aluminum alloy to copper interconnects because of its higher electro migration resistance and lower resistivity, permitting higher clock speed, and lower power dissipation [2]. Copper metalization, however, can never be formed directly on silicon or oxide because of its high diffusivity, which causes degradation of a transistor's operation. Due to this, Ta and TaN films were investigated and used as barrier layers between copper and silicon. Moreover, recent studies showed that a tantalum-nitrite metal gate using low resistivity (~ 15 $\mu\Omega$.cm), bcc(body-centered-cubic)-phase tantalum metal layer is an effective solution to complementary metal oxide semiconductor (CMOS) technology. The TaNx works not only as a buffer layer which prevents tantalum metal films and gate oxide film from reaction with each other but also as a seed layer which helps self-growth of bcc-phase tantalum films [3].

Sputtering is the ejection of surface and near surface atoms caused by the bombardment of energetic ions [4]. It is considered one of several physical vapor deposition (PVD) techniques, which produces thin films from atomic fluxes in a low-pressure gas. For example, it is used to sputter aluminum alloys, titanium, tungsten,

titanium nitride, cobalt, copper and tantalum, which is the material of our interest in this work. Sputtering is the dominant technique used to deposit metallic films in VLSI and ULSI fabrication. The ejection of atoms from the surface of a material is accomplished in the following manner. Initially, a self sustained glow discharge or plasma is ignited at low-pressure gas by applying a large negative voltage to the target. By definition, the target refers to the material to be ion bombarded, which is tantalum in this case, and the substrate refers to the material to be coated; in our application this is gun steel. The low-pressure gas forming the plasma is usually a noble gas like Argon, Krypton or Xenon in order to avoid the reaction with the target material. Plasma consists of charged particles such as positive ions, negative ions, and electrons in a larger pool of neutral atoms and molecules. Positive ions are the most critical to the deposition because they are accelerated toward the target by means of electric fields produced between the substrate and the target. When the energetic positive ions strike the target material, target atoms are ejected from the surface, flying off in random directions. Some of these ejected atoms land on the substrate and subsequently condense, forming thin films.

The main advantage of sputtering deposition is that films of all types: elements, compounds, and alloys including refractory materials, can be deposited by this technique. An important advantage that this technique has over processes like chemical vapor deposition (CVD) is that it can be done at low substrate temperature, one of the reasons it was selected for gun steel substrate. When the tempering temperature of gun steel is exceeded, the mechanical and structural properties of the material can be altered causing gun barrel performance failure [5].

Like any of the existing processes, sputtering deposition has disadvantages. Sputtering requires high capital equipment costs, and it is carried out in low-medium vacuum, which may introduce some undesirable impurities in the thin films. In addition, the characteristics of some films (dielectrics and semiconductors) can be degraded at higher ion energies by X-ray radiation generated from the plasma [6].

Sputtered tantalum exists in two distinct crystallographic forms: a body centered cubic phase (bcc) with a lattice constant of 3.32 A and a metastable tetragonal beta phase with lattice constant of 5.313 A [5]. Bulk tantalum is alpha phase with a room temperature resistivity of 13.6 μΩ.cm. However, there is one report that shows that beta tantalum can be grown in bulk material with a resistivity close 150 μΩ.cm. For gun barrel coating, bcc tantalum is recommended because of its high ductility. Beta tantalum film was found to be highly brittle, thermally unstable, and transforms into bcc tantalum at high temperature (> 750 ^{0}C) conditions [5]. For this reason, it not desirable for the gun barrel coating.

The sputtering process can lead to pure beta, pure alpha or a mix of both phases. Numerous research efforts are oriented toward investigation of the phase formation conditions. So far, the research has shown that numerous parameters appear to influence the crystal structure of tantalum, such as sputtering gas purity, the nature of the substrate surface, substrate bias and temperature during sputtering.

The goal of this thesis was first to investigate different steel substrate surface preparation methods that will serve as the basic foundation for an on going research related to film adhesion properties. Second, to characterize both the structural as well as the electrical properties of the deposited tantalum films on Si, SiO_2, and steel.

The Magnetron sputtering system used in this research and its process control system are described in Chapter 2. In Chapter 3, different surface preparation methods are discussed and the surface roughness measurements of the prepared steel samples using atomic force microscopy (AFM) are discussed. For phase determination, both XRD and Four-Point Probe method has been employed. The four point probe method used for phase film determination on different substrates (Si, SiO2,and steel) is described in Chapter 4. Appendix A contains graph of steel depth in function of particle size grinding compound. Appendix B contains the deposition conditions of all the samples related to this work. Appendix C contains X-ray diffraction lines for alpha and beta tantalum films measured on some of the samples related to this work. Appendix C contains explanation of the curve fitting method.

CHAPTER 2

MAGNETRON SPUTTERING SYSTEM

2.1 Deposition Chamber and Sputtering Source

The vacuum chamber used for sputtering tantalum was designed at the Ion Beam and Thin Film Research Laboratory and made by the Kurt J. Lesker company. The deposition chamber has a cylindrical shape with a total volume of approximately 80 l. The height of the chamber is 15" and the diameter is 20". The top lid of the chamber can be lifted with the help of a motorized hoist. The vacuum chamber was designed to hold from one to four deposition sources for multilayer films. Photographs of the outside and the inside of the sputtering chamber system are shown in Figure 2.1 and Figure 2.2, respectively. The water cooled Magnetron source mounted in the chamber for sputtering tantalum films is a Torus 2, mounted on a tubular support passing through a compression vacuum feedthroug in the chamber's bottom flange. This allows vertical adjustment of the target to sample holder distance. The tantalum targets are 2" in diameter, come in two different thickness, 0.125" and 0.25", and are made of 99.99% pure tantalum.

The sputtering dc power supply can operate in either voltage control or current control mode. The current mode was usually used with the target voltage typically from 250 V to 600 V. The maximum deposition power that was achieved during this work was around 1 kW. A high power resistor (11.4 Ω, 300 W) was inserted in series between the output of the power supply and the sputtering source to control "arcing" phenomena. "Arcing" is the collapse of plasma into small threads of ions and electrons that can be

produced due to particulate contamination of the target surface; insulating contamination on the target; or other source component that might be capable of field emission [7]. When "arcing" is produced during the process, the high energy stored in the capacitors of the power supply is deposited on a small area of the target causing local melting and ejection of particles from the target. The value of the limiting resistor was determined using a circuit simulation software (Pspice) and the limiting resistor was found to be effective in source operation.

To create vacuum, a mechanical pump is first used to evacuate the chamber to a pressure of 100 mTorr. Next, the cryo pump brings down the base pressure to about 8x 10^-8 Torr. During sputtering, working gas is flown to the chamber through mass flow controller and gate valve of the cryo-pump is throttled down to a pressure in 1-100 mTorr range. A turbo molecular pump was recently added to the system for operating with Kr gas which is not effectively pumped by a cryo-pump.

An ionization–type gage measures the high vacuum achieved with the cryo-pump. Durring sputtering the gas pressure is measured with a pressure transducer (MKS Baratron model Type 626) with a range from 0.1 mT-1 Torr.

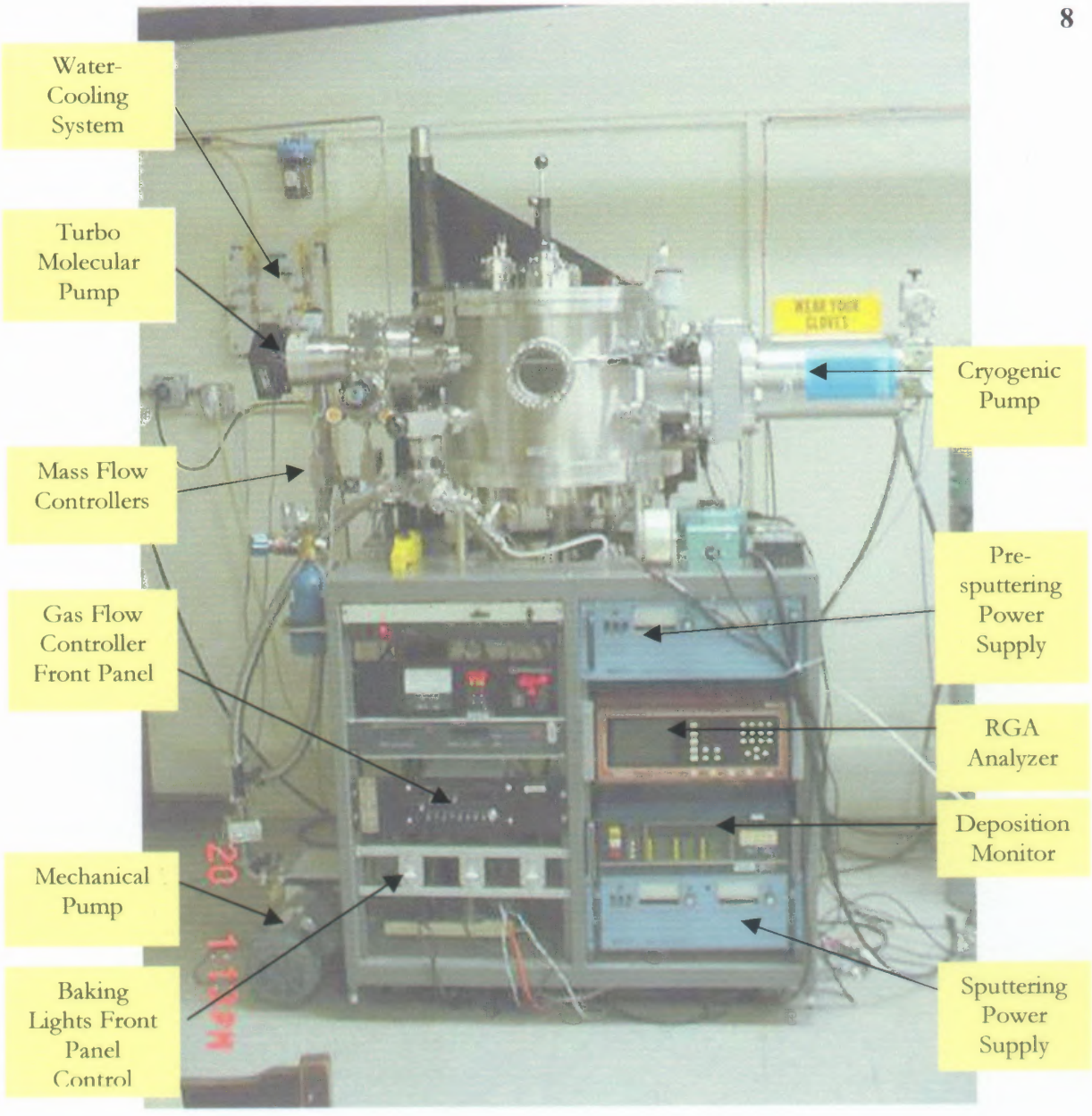

Figure 2.1 DC magnetron sputtering system.

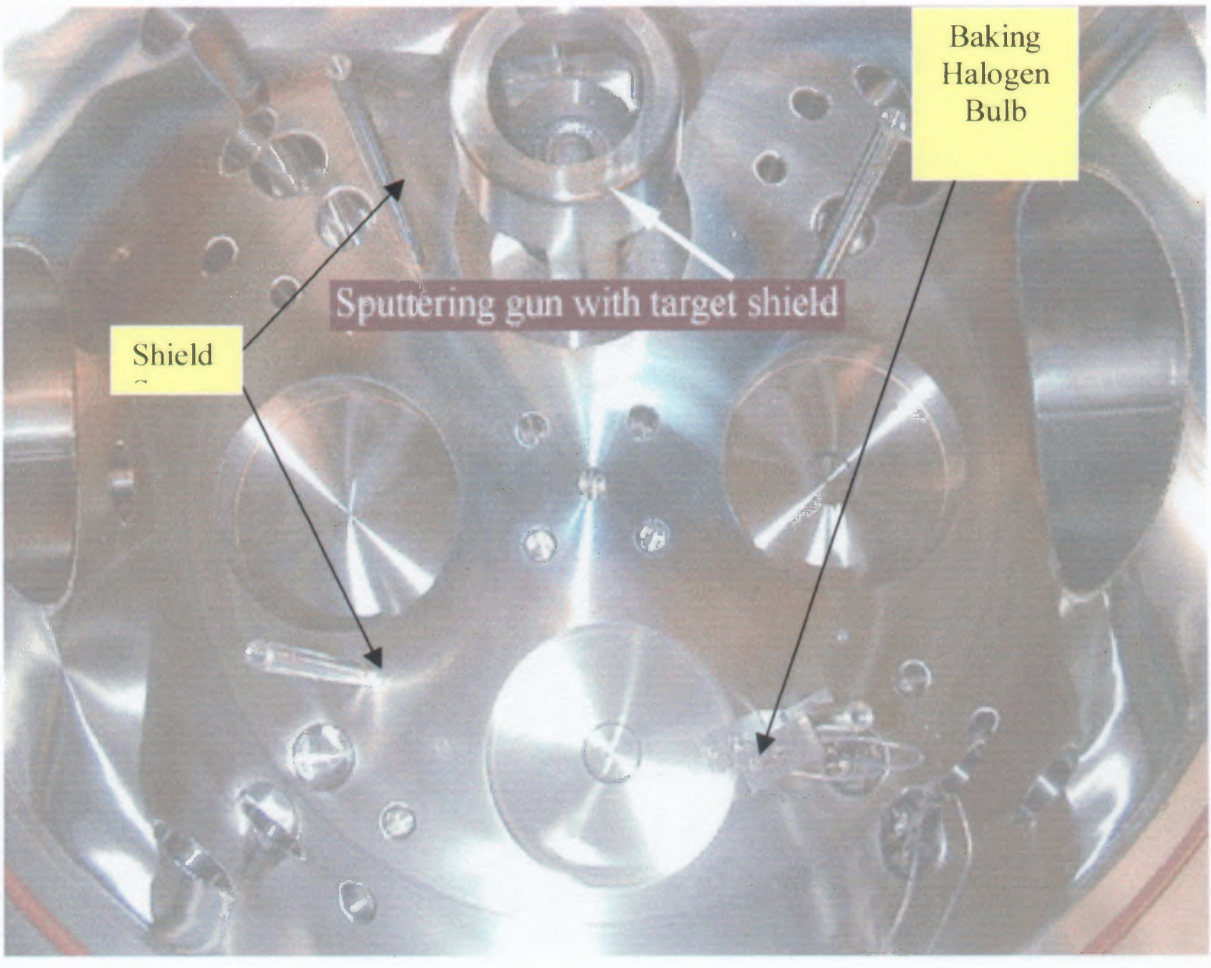

2.2 Substrate and Chamber Heating Systems

For substrate temperature control, a 300 W small halogen bulb with a reflector was mounted on the top lid of the sputtering chamber in such a way that the emitted light is focused by the bulb glass reflector on the top surface of the sample holder. The distance between the bulb and the sample holder is about 2.5 cm. The heat can be applied on all 8-sample holders, as they are positioned above the sputtering source and under the lamp by rotating the substrate platter manually. The substrate temperature can be controlled from 70 ^{0}C (natural process temperature) to 400 ^{0}C using a 0-120AC variac, which is isolated from the system via a 1:1 isolation transformer. More details about the substrate

mounting system are given in the prior master's thesis of Bahvin Shah [8]. Figure 2.3 represents a picture of the substrate heating system.

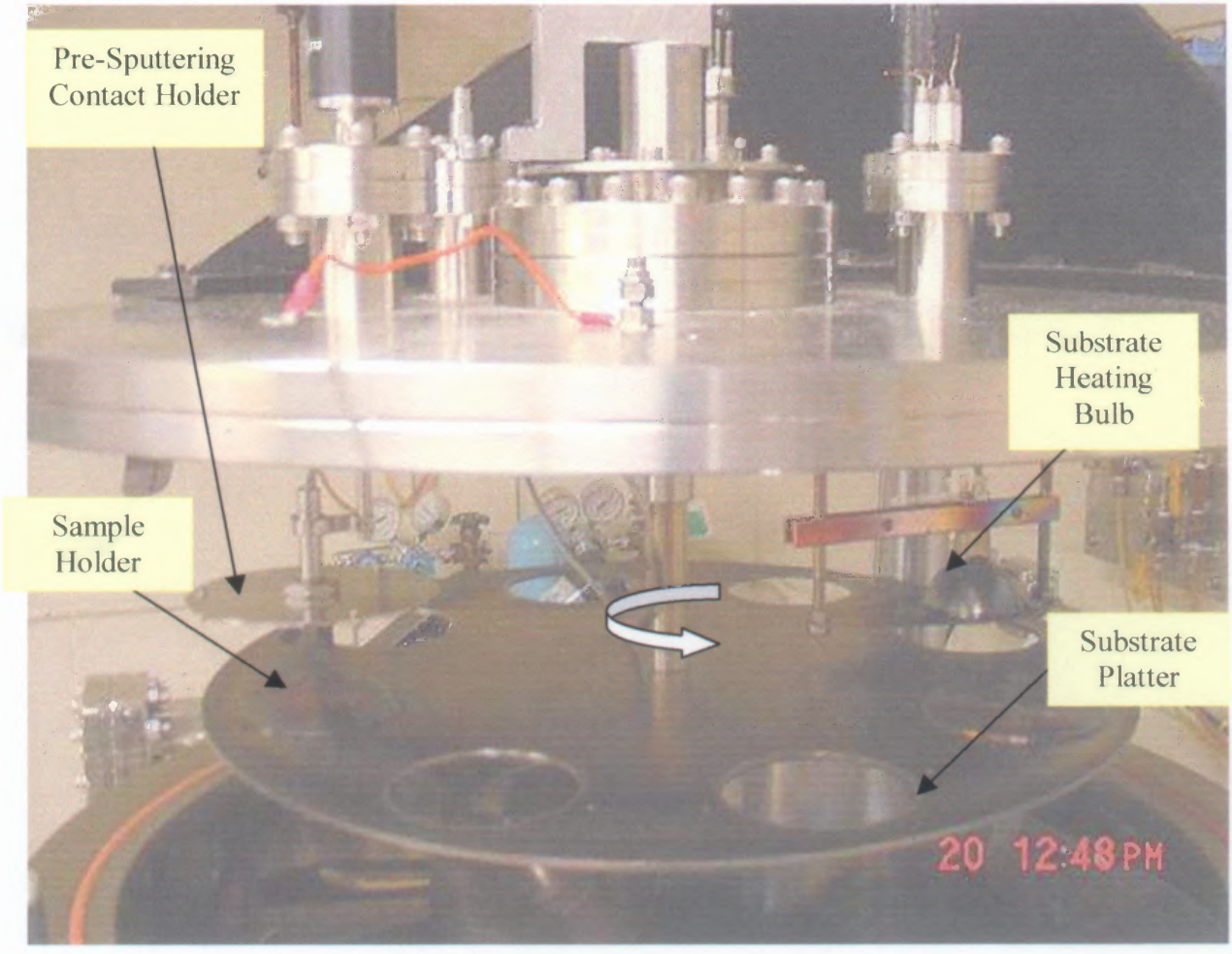

Figure 2.3 A view of the open chamber showing the substrate platter, the substrate heating lamp and the pre-sputtering system. There was no sample holder under the heating lamp in the slot above the sputtering source when the picture was taken.

To reduce out-gassing of the chamber walls after it has been exposed to atmosphere, the chamber was baked under vacuum and subsequently cooled before deposition. Three elongated halogen bulbs (500 W, 120 V) were mounted inside the chamber for this purpose. Two of the bulbs were mounted parallel to the chamber walls,

and the third one was mounted parallel to the lid of the chamber so that the heat distribution was more uniform in the chamber during baking. The baking temperature (up to 250 ^{o}C) was controlled using three Triac based power control boxes mounted on a panel and can be seen in the system's picture in Figure 3.1. One of the baking bulbs can also be seen from the inside view of the sputtering chamber shown in Figure 2.2.

2.3 Substrate Sputter Etching System

Sputter etching of the substrate before deposition can be carried out by applying a negative voltage to the substrate holder by using a vertical linear positioner as shown in Figure 3.4 This is accomplished by lowering a spring loaded connector (shielded by a grounded plate) until it makes contact with the top surface of the sample holder. The sample holder is isolated from the sputtering platter (which is at ground potential) by machined ceramic insulators. A high voltage is supplied through a bnc feed-through (mounted on the lid of the chamber) via a shielded cable. The inner wire of the cable is insulated from the shield by ceramic beads. The sputter etching dc power supply can operate in either voltage control or current control mode. A limiting resistor (10.4Ω, 300 W) was also connected in series between the bnc feedtrough and the output of the power supply for handling "arcing" phenomena.

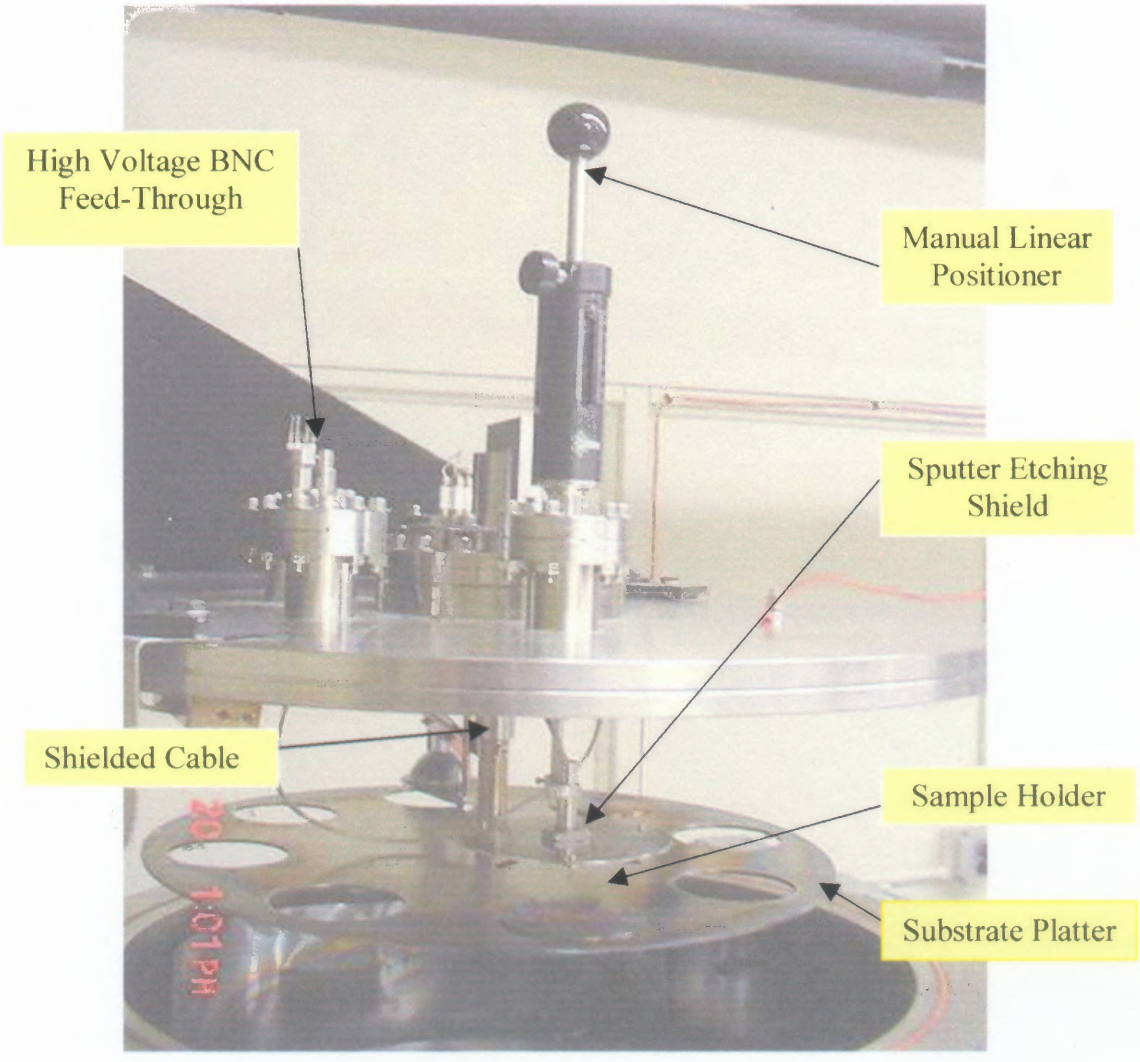

Figure 2.4: Sputter Etching Configuration

2.4 Gas Flow Control and RGA Analyzer System

During sputtering of tantalum, argon or krypton and in some cases nitrogen is released inside the chamber through Mass Flow Controllers. The flow rate of these gases was varied from 1 sccm to 20 sccm and gas pressure, measured by the MKS pressure transducer mentioned previously, was controlled from 24 mTorr to as low as 1 mTorr

with the help of the manual gate valve between the turbo pump and the chamber. The sputtering system is also equipped with a PID controller that can control a motorized gate valve placed between the cryogenic pump and the chamber. More details regarding this mode of pressure control can be found in Mr. Shah's master's thesis [7]. After installation of the turbo molecular pump, manual control with its gate valve for a given gas flow was found to be easy and reliable.

Residual gas was monitored, using an Inficon Quadrex 200 RGA, prior and after the baking of the chamber. Recently, with the installation of a small turbo pump, these measurements were also done during sputtering process. Chamber gas content analysis revealed that before baking, water, nitrogen, and other gases were detected in the chamber due to the atmospheric exposure of the chamber walls and fixtures. After a typical bake of the sputtering chamber, which ranges typically from 6 to 10h, residual gas analysis showed a dramatic decrease of the unwanted gases particularly water vapor. The RGA results before and after backing are presented in the prior master's thesis of Bahvin Shah [8].

CHAPTER 3

Substrate Surface Preparation

3.1 Introduction

Substrate surface preparation is considered one of the most critical steps in thin film technology. It is essential prior to coating, to promote mechanical bonding between the coating and the substrate. Substrate preparation can also influence crystalline properties and other characteristics of the film. The preparation can be done using a number of techniques, such as vapor degreasing, chemical etching, grinding, polishing, etc. [9]. The substrate preparation discussed and investigated in this chapter involves first the planning and smoothing of the sample's surface by grinding and polishing. Second, chemical cleaning of the surface from any incorporated contamination produced by the prior handling of the samples. Third, sputter cleaning by removing contaminated surface layers. The chemical cleaning methods that are applied on the steel substrates are alkaline cleaning, ultrasonic cleaning, and solvent cleaning. Previous studies have found that ion bombardment method combined with chemical cleaning used together allows further improvement of the adhesion properties of thin films [10]. In addition, it was found that for stainless steel, low substrate roughness improves the adhesion of thin solid films [10].

3.2 Mechanical Grinding and Polishing

Gun steel coupons of 12.5 mm by 12.5 mm and 5 mm thickness were prepared by milling and grinding performed in a machine shop. The sample's surface was then ground using a MINIMET Polisher/Grinder made by Buehler Company. Steel samples were ground

using Silicon Carbide adhesive abrasive paper of descending abrasive sizes, starting from 180, and then 240,320, up to 400 grit. Table 3.1 gives the conversion from grit size to particle size based on both FPEA [11] and ANSI [11] standards. Typical grinding parameters such as pressure, sample motion speed, and grinding time were determined both by trial and error and consultation of Sequence B in the MINIMET user guide. Table 3.2 and Table 3.3 present the recipe for grinding and polishing steel alloy respectively.

Table 3.1 Grain Size Designation for SiC Wet-grinding Papers

FEPA standard grit size	ANSI standard grit size	Mean particle size, micron
150	180	95
71	240	71
280	320	52
500	400	35
1000	600	18

Table 3.2 Recipe for Grinding Steel Alloy

Abrasive/Size	Lap	Lubricant	Load[N]	Speed[rpm]	Time[min]
SiC,240 grit	CARBIMET*	DI water	20	25	10
SiC,320grit	CARBIMET	DI water	20	35	10
SiC,400grit	CARBIMET	DI water	20	35	5
SiC,600grit	CARBIMET	DI water	20	35	5

Table 3.3 Recipe for Polishing Steel Alloy

Abrasive/Size	Lap	Load[N]	Speed[rpm]	Time[min]
15 micron	TEXMET*	15	35	5
10 micron	TEXMET	15	35	5
6 micron	TEXMET	15	35	5
3 micron	TEXMET	15	35	5
1 micron	TEXMET	15	35	5
0.5 micron	TEXMET	15	35	5
Gamma Alumina 0.05 micron	MICROCLOTH*	0	25	5

* are products of Buehler Company.

The picture of the MINIMET polisher/grinder in Figure 3.1 shows that the grinder's load arm point is inserted in the back of the sample holder. The sample surface is resting flat against the grinding paper, which is fixed in the stationary bowl. Once the load arm is lowered, exerting some user predetermined force, the sample surface starts grinding against the silicon carbide paper in a flower-shaped pattern shown in Figure 3.2.

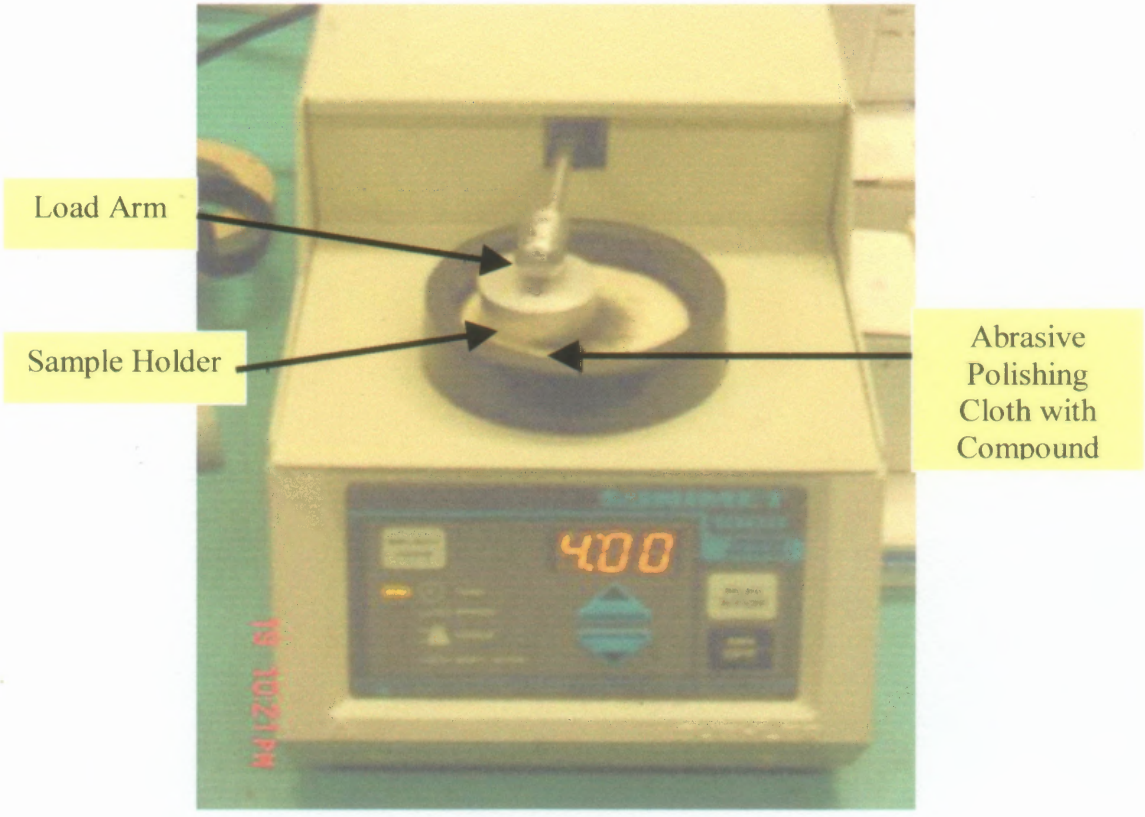

Figure 3.1 Minimet polisher/grinder machine.

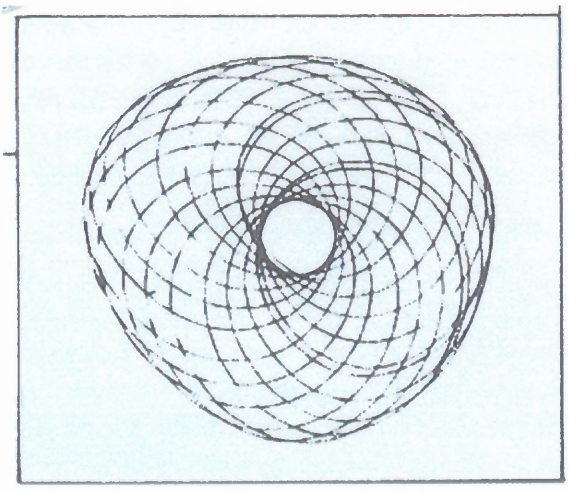

Figure 3.2 Pattern produced by MINIMET polishing action.

One of the features of the grinder is that the sample holder can rotate freely on its own axis while moving on the abrasive paper. That helps to improve the removal rate and to control the grinding and to randomize polishing grooves [12]. Following grinding, polishing was accomplished using the same MNIMET machine. Polishing is essentially the same operation as grinding but with smaller abrasive particles. Suspended diamond particles of descending sizes ranging from 15μ, 10μ, 6μ, 3μ, 1μ, and 0.5μ were applied on cotton-cloth pads during polishing operations. The cotton pad was applied on the glass plate placed in the stationary polishing bowl. Typical polishing parameters such as pressure, rotation speed, and polishing time were determined both by trial and error and consultation of Sequence B excising in the MINIMET user guide; these are included in Table 3.2. Between polishing steps, cleaning of the samples with either Methanol or Acetone was required in order to eliminate any of the diamond particles remaining from previous polishing steps. Final polishing of steel samples was done with Gamma Alumina 0.05μ liquid used on MICROCLOTH pad, giving the steel a shiny, smooth, and nearly scratch-free surface. The advantage of using an Automatic Grinding and Polishing

machine like the MINIMET is that it saves the metallographer time, allows reproducibility by defined working parameters, and often gives a better sample quality regarding flatness and edge retention. Optical microscopy and Atomic Foce Microscopy (AFM) were used to examine the quality of the polishing. These results are presented in section 3.2.3.

3.3 Cleaning of Steel Substrate

The surface cleaning was accomplished by electro cleaning then followed by ultrasonic cleaning. The electro cleaner solution used was "59 Special" made by North West Company. It is described as highly alkaline, and highly fortified with surfactants. The advantage of 59 Special is that it has excellent hard water tolerance, and no drying stains are left on the steel surface. This cleaner removes any oil, grease, shop dirt, fingerprints, or similar films left on the steel substrate surface. The way this alkaline cleaner is used is similar to electro-polishing technique, however the main difference is that the metal is not removed from the work piece, rather it is cleaned. The schematic illustration shown below is a typical electro-cleaning cell where the samples are connected to positive terminal, while the negative (cathode) terminal is connected to a suitable electrode. Copper cathode was used in our laboratory. Both electrodes are submerged into the alkaline solution, forming a complete electrical circuit. A dc power supply used in the system was operated in a constant current mode. The typical operating conditions recommended for the 59 Special solution are tabulated in Table 3.4 below.

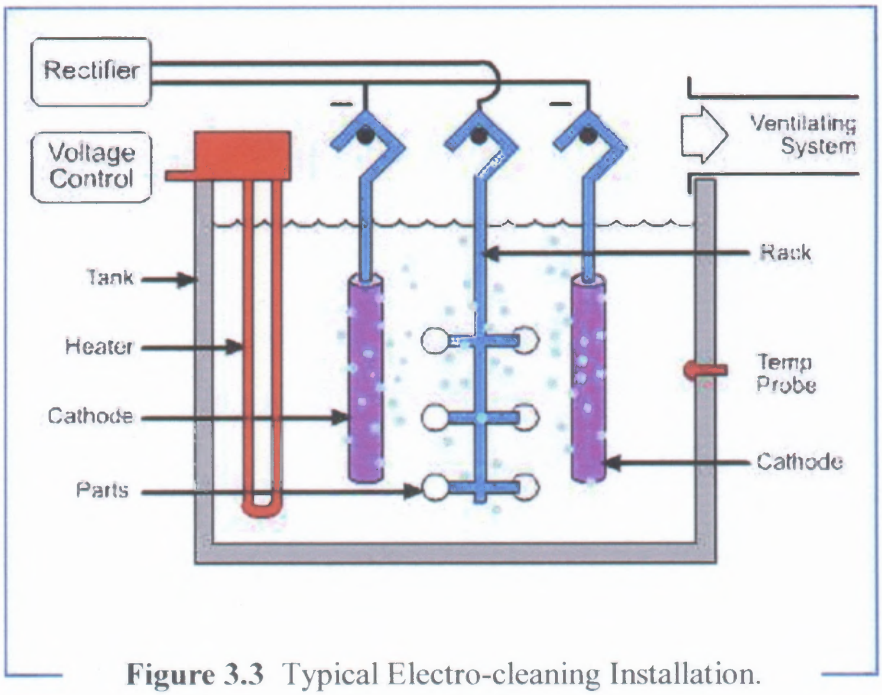

Figure 3.3 Typical Electro-cleaning Installation.

Table 3.4 Operating Conditions with 59 Special Solution

Concentration	8-10 oz/gal. of water(60-75g/l)
Temperature	160-200F(71-93C)
Voltage	6-8 volts
Material to be cleaned	Mild steel
Density	32-54 mA/(cm)^2

After the electro cleaning process was completed, the samples were rinsed in DI water to remove any residual alkaline cleaner. Then, they were carefully immersed into a beaker half filled with Methanol (**CH_3OH**) and placed in an ultrasonic cleaner for 10 min. Next, the samples are removed from the Methanol beaker and transferred to an Acetone (**$(CH_3)_2CO$**) beaker, which is placed in ultrasonic cleaner for 10 min. Finally, the samples were cleaned ultrasonically in Methanol for another 10 min and dried. The cleaned samples were kept in a dessicator in order to prevent any corrosion.

3.4 Sputter Cleaning of Steel (Etching)

Sputter etching is a technique used to remove surface layers prior to film deposition. Energetic ions (extracted from plasma) eject atoms of the sample's surface by transferring their momentum, consequently removing very thin top surface layer of the material. This method was found to be one of the most effective method in PVD process for improving the adhesion of thin films [11]. However, this cleaning method is known to have some negative effects on substrates, which includes backscattering, redeposition, cone formation and surface contamination due to residual gases [12].

Steel samples were first polished with 0.5μm diamond particles and cleaned by acetone and propanol in an ultrasonic cleaner as described previously. Then, the steel samples were sputter- etched using argon gas of pressure of 85-168.7 mTorr for 30 to 45 min. The flow of argon gas was 18 sccm and the sputtering voltage was 550 V. Prior to sputter etching, residual gases in the chamber were minimized by baking and then cooling of the chamber under high vacuum. AFM measurements of the surface of theses samples are described in section 3.2

3.2 AFM Measurements of Steel Substrate Surface

3.2.1 Introduction

Atomic Force Microscopy (AFM) is one of the material characterization techniques commonly used for surface investigation. It is capable of producing a three-dimensional surface topology at nanometer lateral and sub angstrom vertical resolution. This method can be used both on insulators and conductors, which makes it very attractive for surface imaging of various materials. During measurement, a sharp probe tip is scanned over a

sample surface and follows its topography. The deflection of the arm holding the tip is used to form a high-resolution image. The AFM instrument used for our investigation is a Nano-Scope IIIa made by Digital Instrument; it is available through NJIT's Environmental Engineering (York Center). This Nano-Scope is capable of scanning up to 152μ by152μ horizontal area and 5μ vertically.

3.2.2 Description

AFM measurement consists of scanning a sharp tip across a sample surface while maintaining a small, constant vertical force. These forces can range from 0.1 to 100 nN.

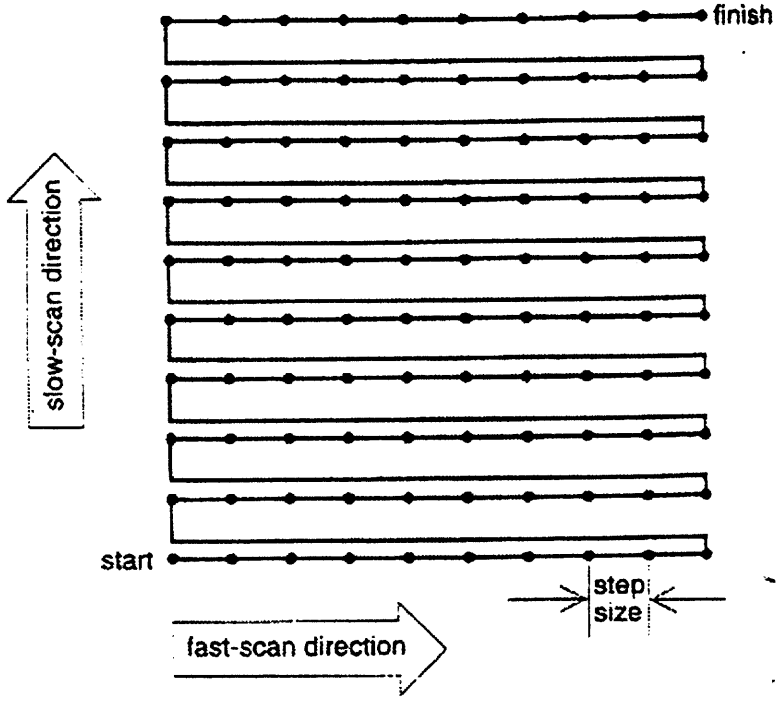

Figure 3.4 Picture of AFM raster pattern.

The tip, mounted on the end of a flexible cantilever is a few microns long and less than 10 nm in diameter. The scanning motion is effected by a piezoelectric tube, which

manipulates the sample in a raster pattern with respect to the fixed tip. Figure3.4 represents a typical scanner motion.

The tip-sample interaction is monitored by reflecting a laser beam off the back of the cantilever into a split photodiode detector. By sensing the difference in photodiode output voltages, changes in the cantilever deflection or oscillation amplitude are determined. A schematic of this arrangement can be seen in Figure 3.5.

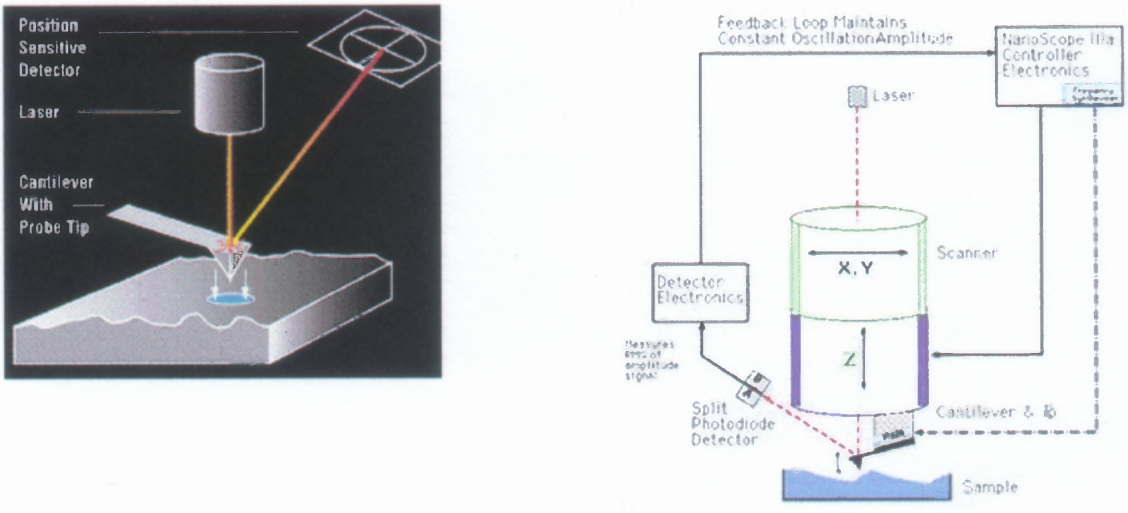

Figure 3.5 Schematic and block diagram of the AFM.

AFM can be used in four modes:

- Contact mode
- Tapping mode
- Electric mode
- Magnetic mode

However, since the contact mode AFM and the tapping mode AFM are the most useful modes in this study, we will limit our discussion to these two. The NanoScope user manual is a good source for further information on the different AFM modes that are available.

Contact mode:

Contact mode AFM consists of scanning the tip in contact probe with the surface while monitoring the change in cantilever deflection with the split photodiode detector. A feedback loop maintains a constant cantilever deflection by vertically moving the scanner to maintain a constant photo detector difference signal. The distance the scanner moves vertically at each x, y data point is stored by the computer to produce the topographic image of the sample surface. The force is computed from Hook's Law: $F = k*x$ where

- F: Force
- K: spring constant
- x: cantilever deflection.

The advantage of contact mode is that it provides higher scan speeds (throughput), and produces "atomic resolution" images. The disadvantage is that lateral (shear) forces can distort features in the image and can damage soft samples, or damage the tip due to friction between tip and sample.

Tapping mode:

Tapping mode AFM consists of oscillating the cantilever at its resonance frequency (typically~300 KHz) while lightly "tapping" on the surface during scanning. The laser deflection method is used to detect the root-mean-square (RMS) amplitude of the cantilever oscillation. A feedback loop maintains a constant oscillation amplitude by moving vertically at every x, y data point. Recording this movement forms a topographical image. The advantage of tapping mode over contact mode is that it eliminates the lateral, shear forces present in contact mode. This enables tapping mode to image soft, fragile, and adhesive surfaces without damaging them.

Overall, AFM is a high-resolution imaging instrument that can be used effectively to study surface properties of materials. In our case, AFM was used to examine the steel surface after being submitted to different preparation methods. In addition, it was used for our thin film surface investigation to determine changes in morphology with variation of the deposition process control. However, the AFM image is affected by the instrument characteristics and may have distortions due to nonlinearity, hysteresis, and aging of the piezoelectric stage. Additionally, the wear of the diamond tip can affect the interaction between the tip and the surface For example, deep features on the surface will not be probed properly because of the tip sharpness loss.

3.2.3 AFM Measurement On Steel Substrates

AFM contact mode analysis was conducted on the steel coupons prepared by mechanical grinding and polishing methods, which were discussed previously. A 100 μm by 100 μm scan area was accomplished on samples ground by 320grit, 400grit and the ones polished by 6μm, 3μm, 0.5μm and 0.05μm paste. Roughness parameters were calculated from the scan height picture of the samples. From the AFM images presented from Figure 3.6 to Figure 3.11, grinding effect using 320grit and 400grit and smoothening effect using different diamond particle sizes were noticed on the sample surface. The smaller the diamond particle size the smoother the steel. However, the polishing procedure left small pits in the substrate surface polished with 0.5 μm [5]. After using Gamma Alumina for final polishing it seems that the small pits were eliminated; this can be seen in Figure 3.11. The mean roughness (Ra) of the scanned 10000 μm^2 area was calculated with a statistical software tool, which comes as part of the imaging software. The mean roughness was defined by the ASME B46.1 standard available from the American Society of Mechanical Engineers as the following:

Mean Roughness (Ra): Arithmetic average of the absolute values of the surface height deviations measured from the mean plane within the area selected by the user; in our case both 100 μm by 100 μm and 30 μm by 30 μm:

$$Ra = (1/N) \times \Sigma |Zj| \text{ from } j=1 \text{ to } N.$$

Table 3.5: Mean Roughness of Polished Steel Measured by AFM

Abrasive	Ra for 100 μm x 100 μm scan area in [nm]	Ra for 30 μm x 30 μm scan area in [nm]
SiC, 320grit	88	65
SiC, 400grit	46.7	42
3 μm	8.63	7.9
1 μm	15.4	8.9
0.5 μm	37	6.5
0.05 μm	12.9	5.1

The roughness after the final gamma alumina polishing was found to be around 5 nm for 30 μm x 30 μm scan area. The results show that the mean roughness of the surface is approximately one order of magnitude smaller than the size of the abrasive particle used for polishing. This is in agreement with graph in Appendix A. Due to surface abnormalities caused most likely by surface contamination from mishandling of the samples, roughness value for 3 μm was found to be less than the one for 1 μm.

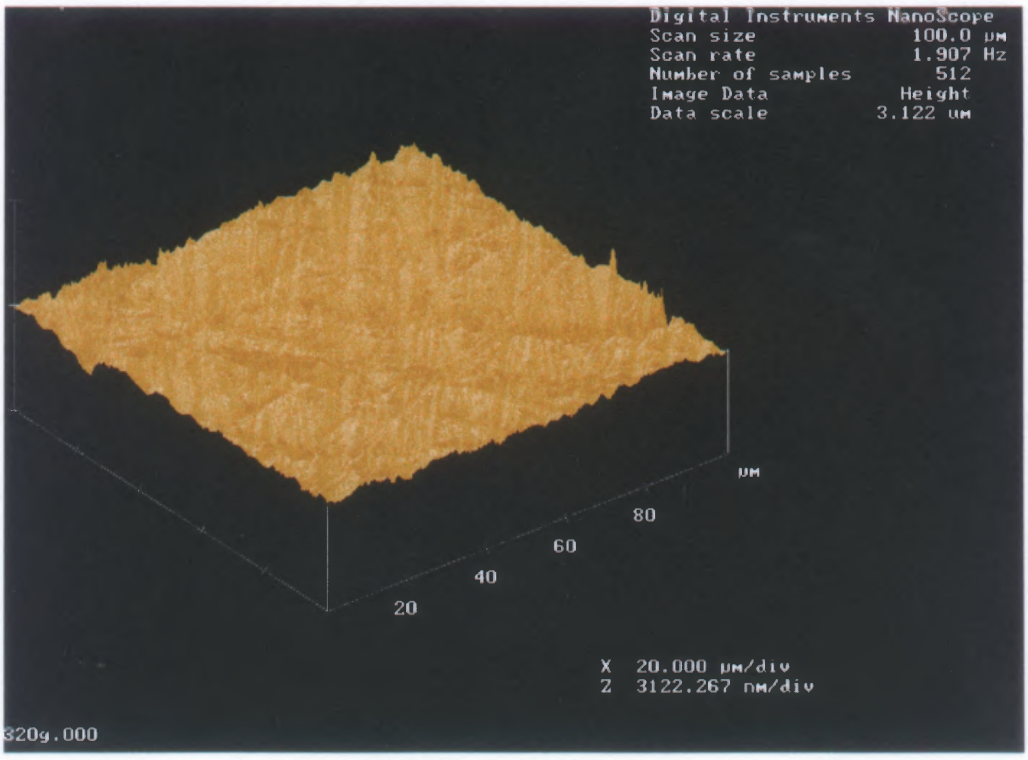

Figure 3.6 Steel surface image polished with 320 SiC grit.

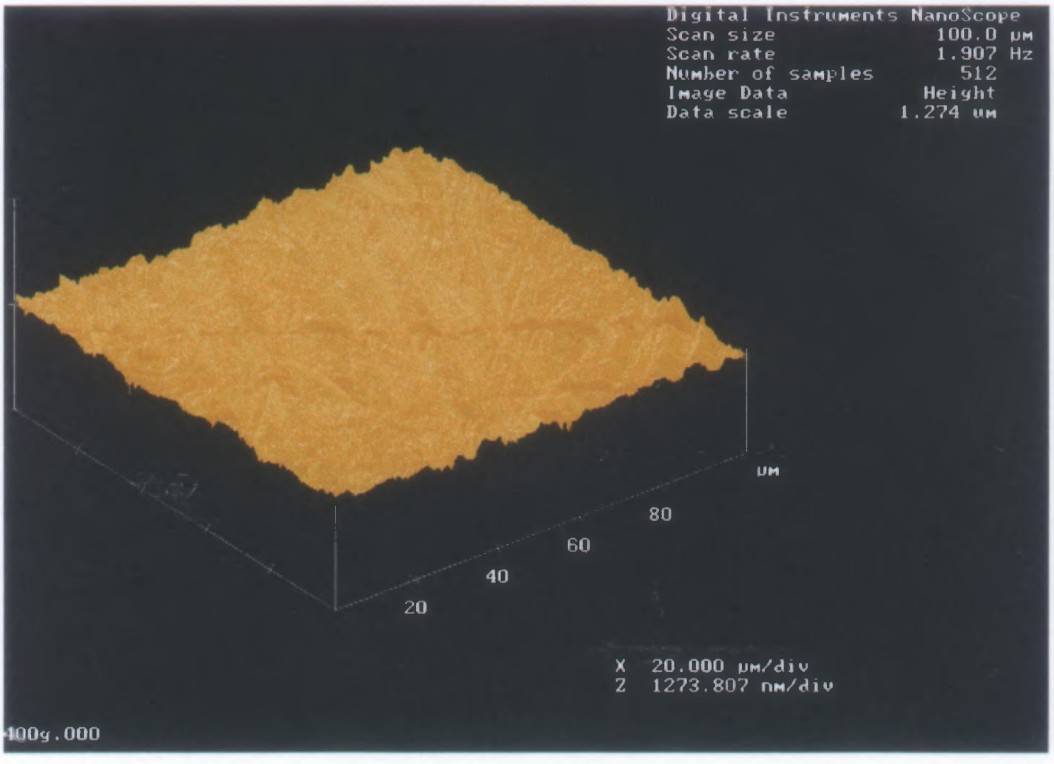

Figure 3.7 Steel surface image polished with 400 SiC grit.

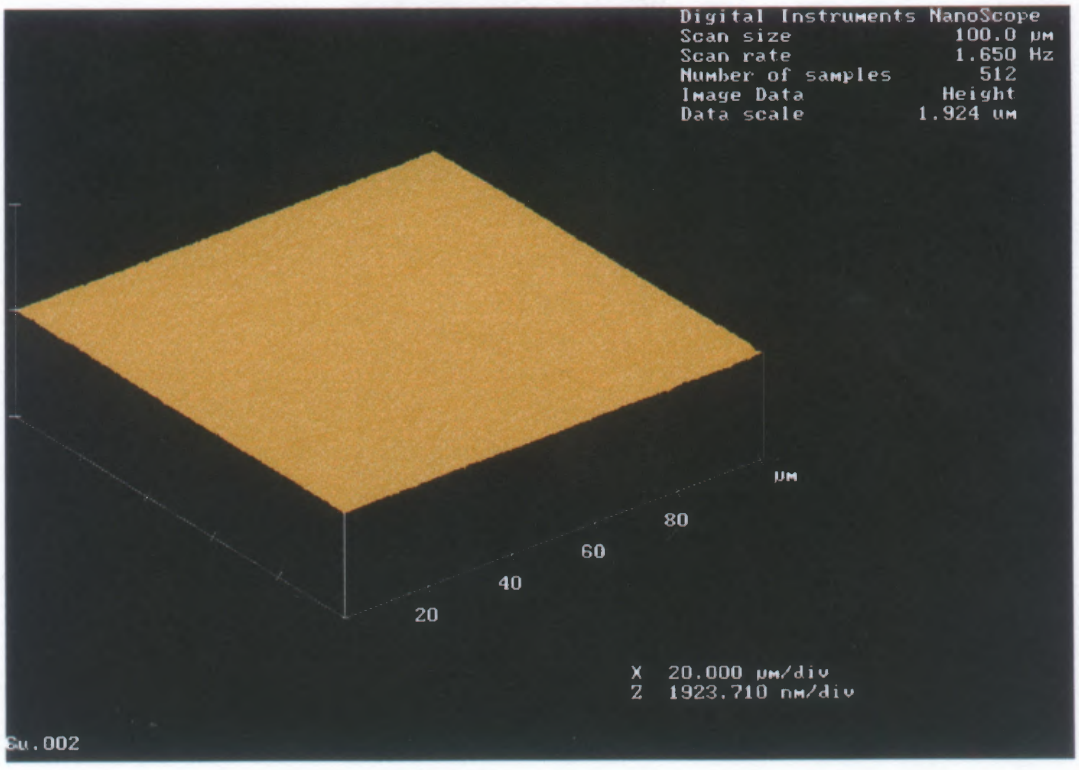

Figure 3.8 Steel surface image polished with 6 µm diamond paste.

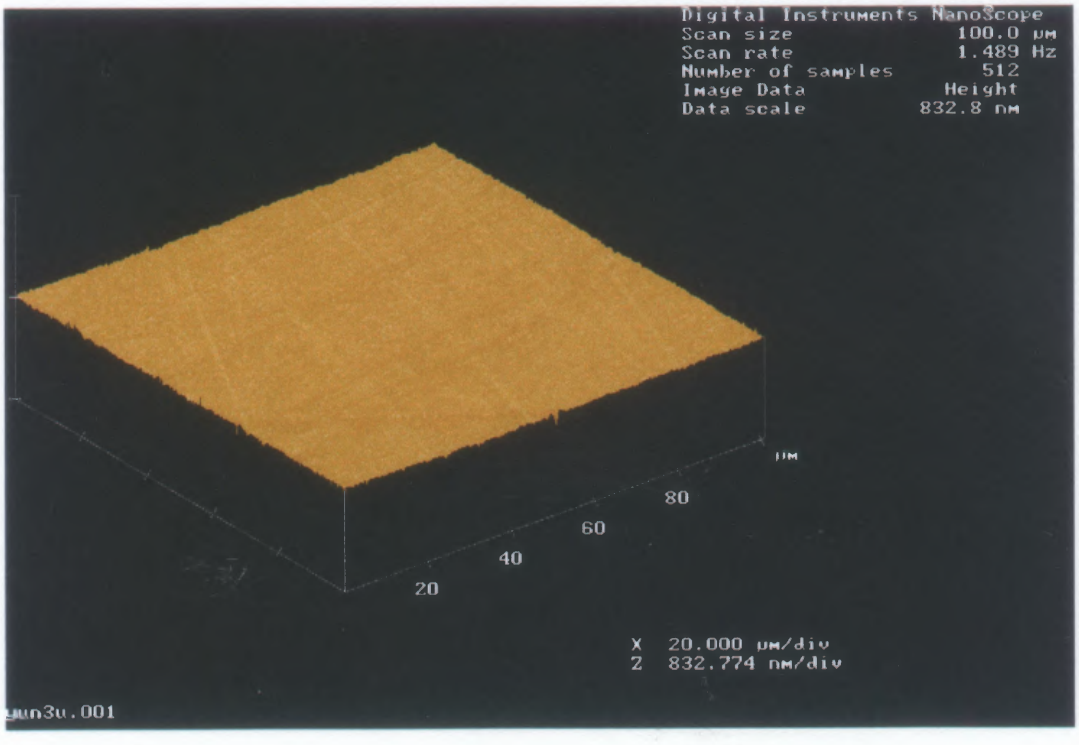

Figure 3.9 Steel surface image polished with 3 µm diamond paste.

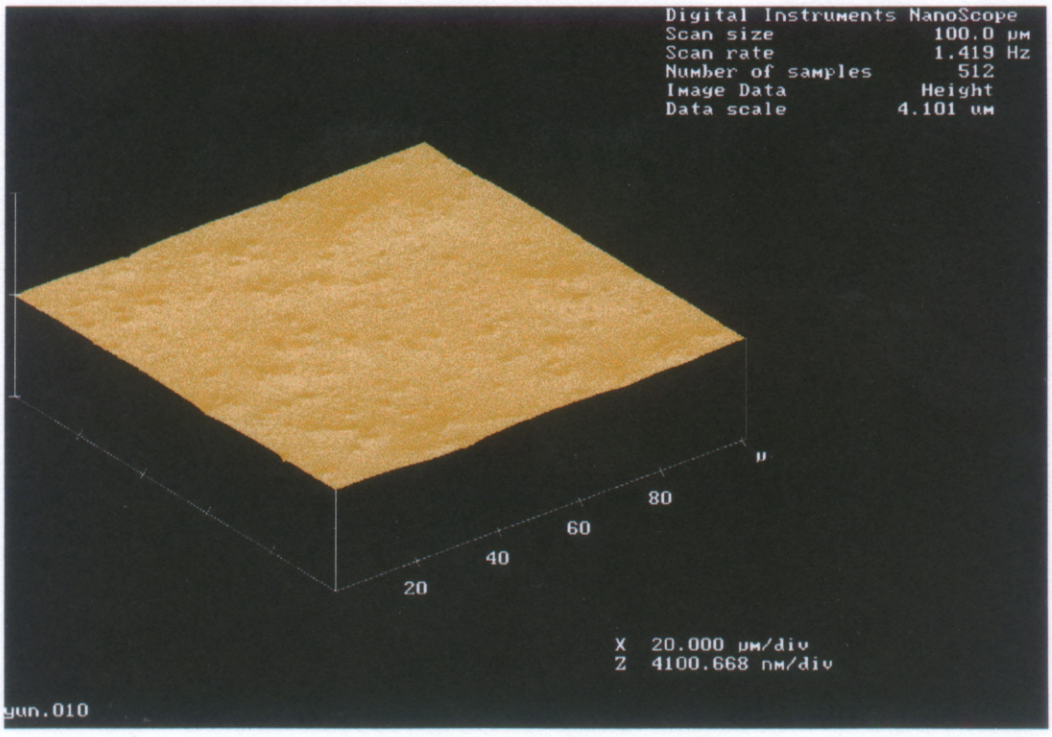

Figure 3.10 Steel surface image polished with 0.5 µm diamond paste.

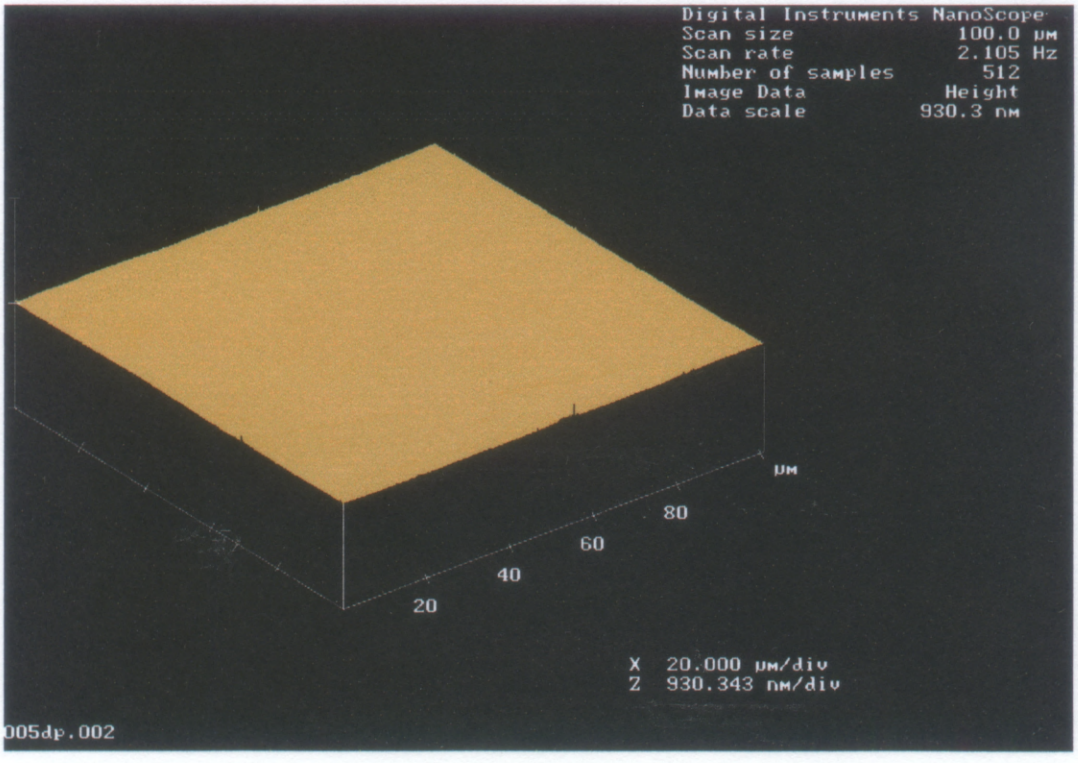

Figure 3.11 Steel surface image polished with 0.05 um alumina paste.

AFM measurements were also done on the sputter-etched steel substrates and the resulting topology images are shown below from Figure 3.12 to 3.14. The steel substrates were polished with 0.5 μm diamond paste prior to sputter-etching.. Sputter etching was done for 45 min with argon of 85-168.7 mTorr pressure and 550 sputtering voltage. The measured average roughness Ra for sputtered-etched steel substrates is 6.5 nm (for 30 μm x 30 μm scan area) which is same as 6.5 nm starting roughness, shown in Table 3.5. The sputtering-etching process is expected to increase the starting roughness of steel substrate, but that was not the case for our sample. It has been reported that the effects of sputter-etching process on steel substrates reduces with the increase of the sputter-etching time [13]. In addition, the greatest improvement in adhesion is expected for shorter sputter-etching time [13].

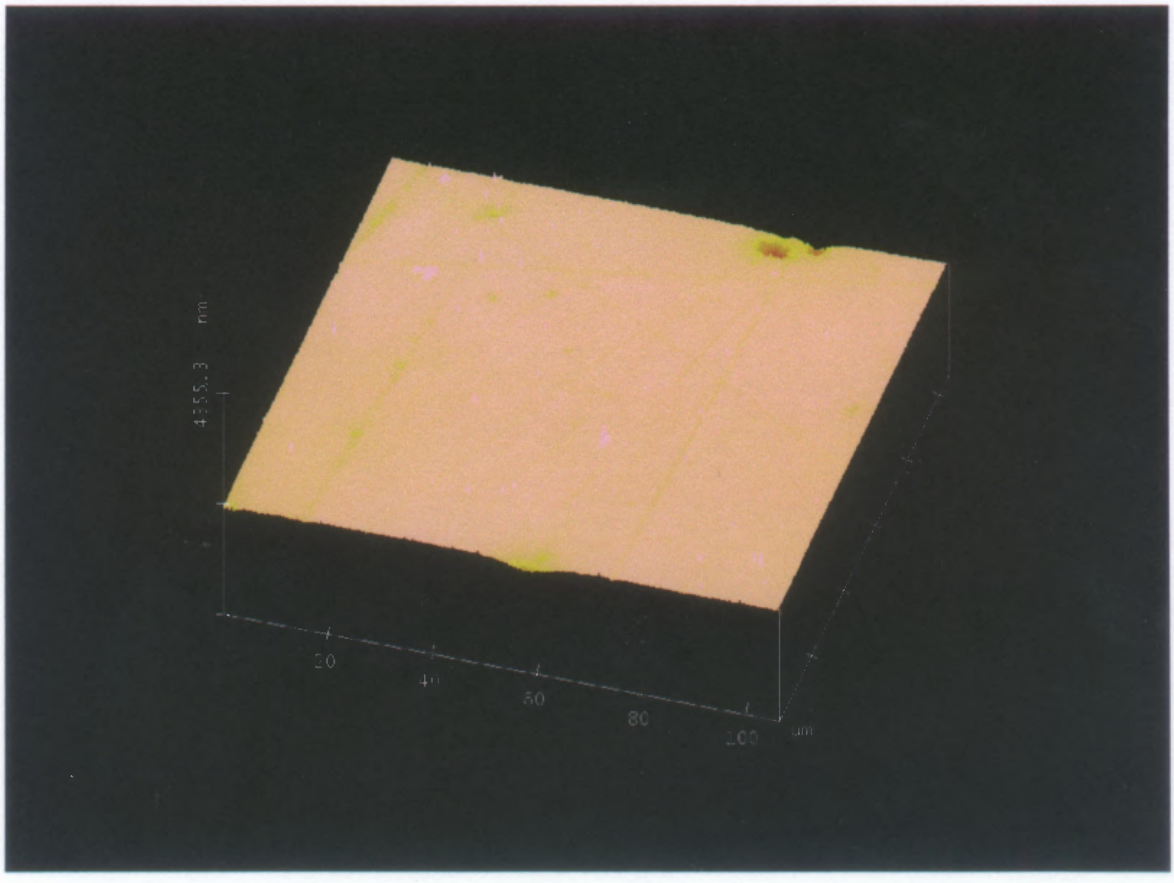

Figure 3.12 Steel surface image sputter-etched using argon.

Surface morphology of steel was found to be different from area to area on the steel substrate. Formation of cones was noticed on some areas of the steel surface and is shown in Figure 3.13. Cone formation was first observed by Whener, Hajicek and Vossen [13] on different metals like Cu and Pd. It was shown that the cone formation was due to local masking effect by impurities. Because of the lower yield of the contaminant than from the substrate surface, the substrate material around the impurity was sputtered away faster [13].

In some areas of steel surface larger protrusions of the steel substrates were found, as shown in Figure 3.13.This may result from re-sputtering of materials that has condensed on another surface; and electrostatic attraction of emitted posited ions [13].

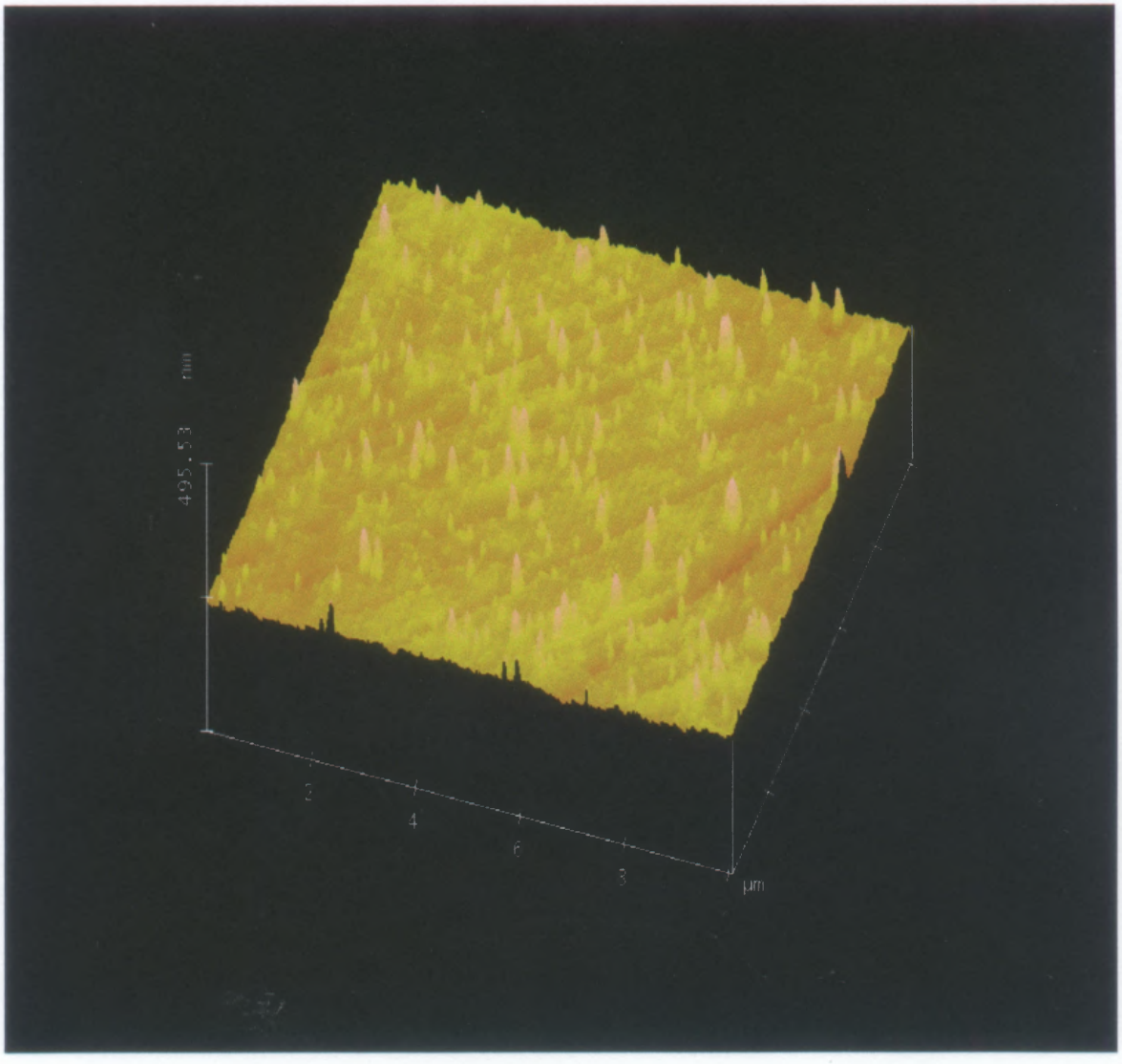

Figure 3.13 AFM image of 10 um by 10 um of sputtered-etched steel surface.

Metallic flakes due to sparking were observed on some area, as shown in Figure 3.14.

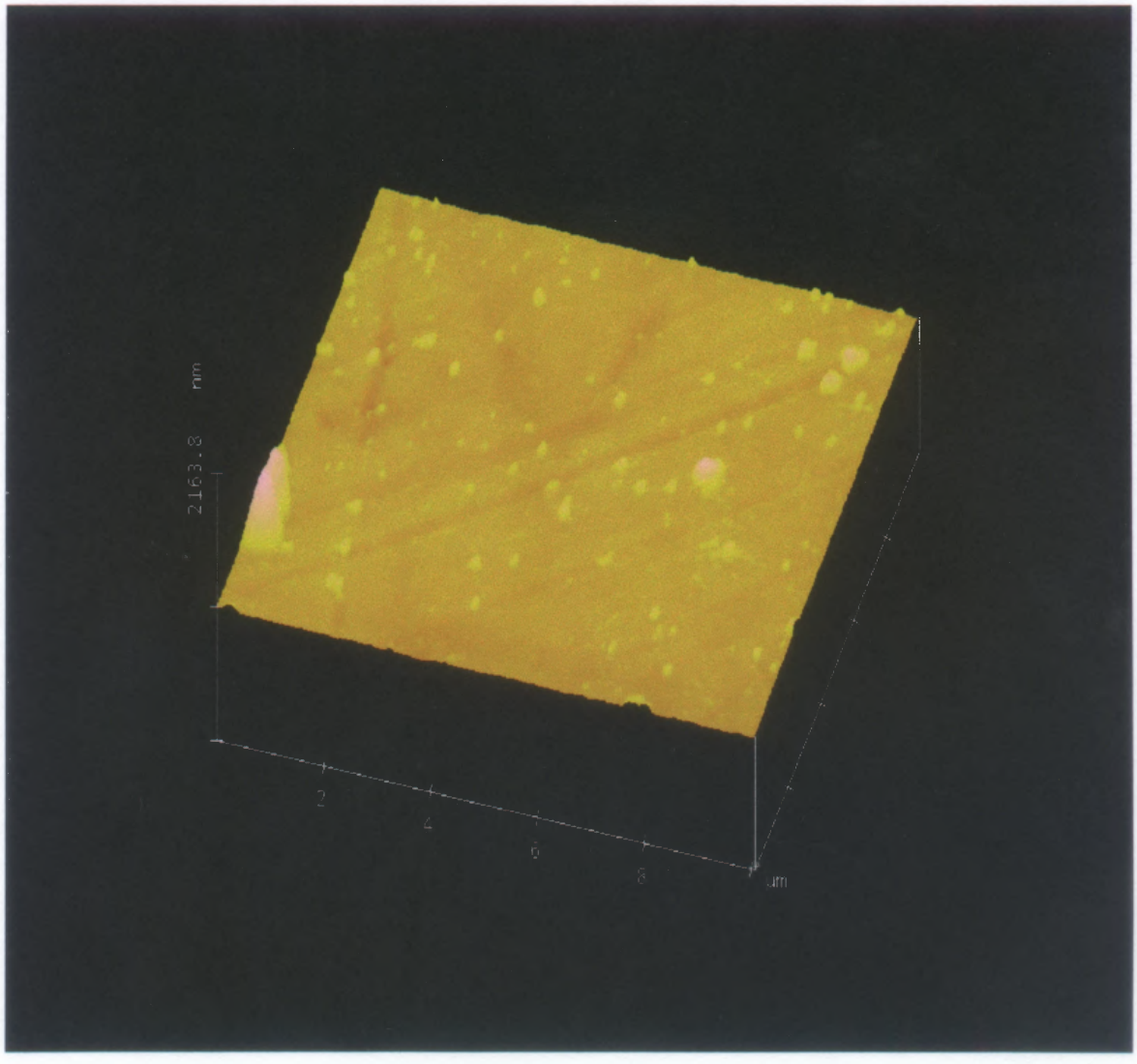

Figure 3.14 AFM image of 10 um by 10 um of sputtered-etched steel surface.

CHAPTER 4
CHARACTERIZATION OF TANTALUM FILMS BY RESISTIVITY MEASUREMENT

4.1 Introduction

The Four-Point Probe is a tool for measuring the resistivity of a material by contact with its surface. The tool is widely used in the semiconductor industry and has applications in both manufacturing and research. In semiconductor processing, it is used to determine the acceptance requirement for silicon and gallium arsenide wafers. In addition, it is used to characterize metalization interconnect layer and to measure the resistivity of different Si layers doped with impurities like boron and arsenic.

The tool consists of four spring loaded sharp point probes (typically made from gold or tungsten carbide) put in an in-line configuration with equal spacing. The outer two probes are current probes and the inner two probes are voltage probes. The schematic of the in line-four point probe is provided below in Figure 5.1. A low current (typically up to 150 mA), generated by a low output impedance current source, is injected through one of the current probes and extracted from the other, while the voltage across the voltage probes is sensed by a high input impedance voltmeter. Due to the separation of the current probes and the voltage probes, the voltage measured is essentially independent of contact resistance; this is why the four-point probe is chosen over the two-probe method. The resistivity of a material is computed by multiplying the ratio of measured differential voltage over injected current by a correction factor accounting for geometrical effects related to thickness, sample shape, sample edge effect, and sample diameter. The details are given in the following section.

The advantages of the four-point probe is that it is a relatively easy to operate and powerful diagnostic tool. The disadvantage of this method is that when the probe tips come in contact with the material, surface indentation patterns might be left on the surface or scratches due to accidental lateral movements, causing some material damage. The probe also samples a relatively large area of the material and is not suitable for high special resolution measurements.

In the following sections the theory of four-point probe, including geometric factor, is reviewed and the results of resistivity measurements on different phase tantalum films are presented. The objective behind the study of the four-point probe method in this work is to explore its ability to determine the phase composition of the tantalum films. XRD measurements were conducted to confirm the validity of the Ta phase determination by the four- point probe measurement.

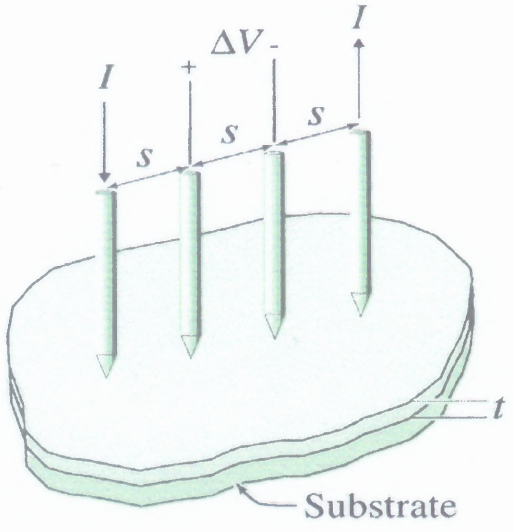

Figure 4.1 In Line Four Point Probe configuration [14].

4.2 Four-Point Probe Theory

The resistivity of an arbitrarily shaped material is related to the resistance or the differential voltage current ratio, and the correction factors. It's generally represented by [15]:

$$\rho = 2 \cdot \pi \cdot s \cdot F \cdot \left(\frac{\Delta V}{I} \right) \tag{4.1}$$

where:

- ΔV: measured differential voltage.
- I: injected current.
- F: correction factor.
- s: probe spacing.

For measurement on a sample for which the lateral extent is much greater than the probe spacing, the correction factor, F(s,t),depends **only** on the spacing and the sample thickness. Normally there are other correction factors that should be taken under consideration, like the effect of the placement of the probes relative to the sample edges [16], and sample lateral dimensions [16]. However, their effects in samples used in this work are so small compared to the effect of thickness and spacing that they will be neglected in the following review. The papers related to resistivity, listed in the references section, give more information regarding different correction factors, especially the paper by Valdes [16].

The solution for the resistance measured by four-point probe including its correction factor, was described previously by authors who used the method of images [16] and Fourier-Bessel functions [17] [18] [19]. Recently, Weller published a paper where he developed an accurate algorithm for the computation of the theoretical values of the four-point probe thickness correction factors using a Euler- Maclaurin expansion [14].

Some of his results are presented her along with the results of Albert and Berkowitz, which are easy to implement in measurement applications, but less accurate.

The four-point probe resistance was proven to be independent of the probe current density and the probe radius [17][18] [19]. By solving Laplace's equation for one layer analysis using Fourier-Bessel approach, $Z\ (t,\ s) = (\Delta V/I)$ was derived for two specific cases and their results are the following:

1. Uniform Resistivity Layer over Perfectly Insulating Boundary:

$$Z(t,s) = \frac{\rho}{\pi} \cdot \int_{\frac{1}{2 \cdot s}}^{\frac{1}{s}} \coth(\lambda, t) \cdot d\lambda = \frac{\rho}{\pi \cdot t} \cdot \ln\left\{ \frac{\sinh\left(t/s\right)}{\sinh\left(t/2 \cdot s\right)} \right\} \tag{4.2}$$

Where:

- ρ : Resistivity of top layer
- t: Top layer thickness
- λ: Integration variable
- s: Probe spacing

For t/s << 1

$$Z(t,s) = \rho \cdot \frac{\ln(2)}{\pi \cdot t} \tag{4.3}$$

since the limit of the ratio of the hyperbolic sin functions approaches 2 when (t/s) approaches zero.

For t/s >> 1

$$Z(t,s) = \frac{\rho}{2 \cdot \pi \cdot s} \tag{4.4}$$

since the limit of the logarithm of the ratio of the hyperbolic sin function go to ½ when (t/s) goes to infinity.

2. Uniform Resistivity Layer over "Conducting" Boundary:

$$Z(t,s)=\frac{\rho}{\pi}\cdot\int_{\frac{1}{2\cdot s}}^{\frac{1}{s}}\tanh(\lambda,t)d\lambda=\frac{\rho}{\pi}\cdot\ln\left\{\frac{\cosh\left(t/s\right)}{\cosh\left(t/2\cdot s\right)}\right\} \tag{4.5}$$

It very important to understand that "**Conducting**" means the substrate resistivity can be neglected in comparison with the overlying film. The following relations are based on that understanding:

For t/s << 1

$$Z(t.s)=0 \tag{4.6}$$

since the limit of the logarithm of the ratio of the hyperbolic cos functions approaches zero when (t/s) approaches zero.

For t/s >> 1

$$Z(t,s)=\frac{\rho}{2\cdot\pi\cdot s} \tag{4.7}$$

since the limit of the logarithm of the ratio of the hyperbolic cos functions go to 1/2 when (t/s) approaches infinity .This is the same results as for case 1.

Weller deduced from his "**conducting**" substrate geometric factor F_{12} in equation 4.1, that when the film is thicker, the resistivity of the substrate becomes irrelevant [14]. However, when the film is thin on a conducting substrate, current is shorted by the substrate. Thus, as the film thickness decreases, the sensed differential voltage produced by the injected current rapidly approaches zero.

The question that rises in this case is what is the minimum film thickness to generate some sensible four-point probe measurements. Weller suggested according to his results that for (t/s) = 0.2, the four-point probe resistance can be measurable. For example, for a 0.5 mm probe spacing we could detect the resistivity of 100 μm thick film. Therefore, the smaller the

probe spacing the more sensible the resistivity method gets. The thickness correction factors F_{11} and F_{12} for both insulating and "**conducting**" substrates ,respectively computed by Weller are shown in Figure 4.2 as a function of $\tau=t/s$.

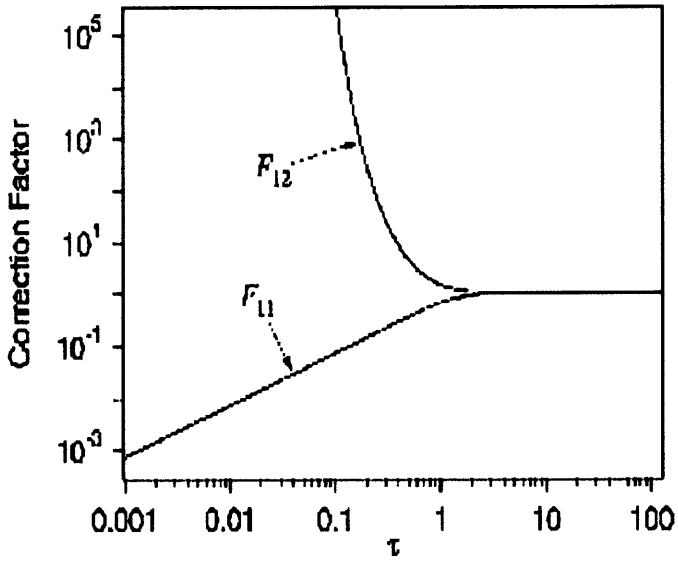

Figure 4.2 Thickness correction factors F_{11} (insulating substrate) F_{12} (conducting substrate) versus $\tau=t/s$ [14].

For resistivity case where the substrate value of *Z(t,s)* minus the surface value of *Z(t,s)* is significant [17], meaning that when the substrate resistivity is very high compared to the film resistivity, the effect of the substrate can be eliminated. This can be denoted by the equation:

$Z = Zeff\ Zs/(Zeff+Zs)$

Where:

- Zeff: (ΔV/I) of film on insulating substrate
- Zs: (ΔV/I) of substrate.

Sunde developed basic theory for earth's resistivity in his book [20]. He derived mutual resistance (ΔV/I) formulas for the case of two-layers with uniform resistivity. He extended his model to three-layers and then gave a general expression for the case of n-layers. Sunday's work will be adopted for our film resistivity measurements.

For resistivity case where the substrate resistivity happen to be different than the overlaying film, the resistivity is represented by [20]:

$$\rho = \frac{2 \cdot \pi \cdot s}{f(\tau, \alpha)} \cdot \left(\frac{\Delta V}{I} \right) = 2 \cdot \pi \cdot s \cdot F(\tau, \alpha) \cdot \left(\frac{\Delta V}{I} \right) \tag{4.9}$$

Where $F(\tau, \alpha) = \frac{1}{f(\tau, \alpha)}$ and $\alpha = \rho_{substrate} / \rho_{film}$

The correction factor is expressed not only as function of the ratio of the thickness to the probe spacing τ = s/t, but also as a function of the ratio of the film resistivity to the substrate resistivity $\alpha = \rho_{substrate} / \rho_{film}$. When the probe separation is small compared to the thickness of the film the measured potential difference is hardly influenced by the boundary (substrate) since its distance is large compared with the probe spacing. As the probe spacing is increased the depth of investigation increases and with it the influence of the lower layer[21].

The inverse correction factor $f(\tau,\alpha)$ for four-point probe method can be determined in function of the inverse correction factor for two-point probe method f_0 (τ,α) and it is expressed as:

$$f(\tau,\alpha) = 2 \cdot f_0(\tau,\alpha) - f_0(2 \cdot \tau,\alpha) \tag{4.10}$$

Where

- f (τ,α): Inverse correction factor for four-point probe method.
- f_0 (τ,α): Inverse correction factor for two-point probe method.
- α: Substrate resistivity to film resistivity ratio.
- τ: Probe spacing to film thickness ratio.

The (ΔV/I) or what Sunde called mutual resistance for tow-point probe method (for two-layer structure) was derived as [20]:

$$\frac{\Delta V}{I} = \frac{\rho_{FILM}}{2 \cdot \pi} \cdot \int_0^{\infty} \frac{1 - \mu_1 \cdot e^{-2 \cdot \lambda \cdot t}}{1 + \mu_1 \cdot e^{-2 \cdot \lambda \cdot t}} \cdot J_0(\lambda \cdot s) \tag{4.11}$$

Where:

- J_0 : First order Bessel function
- $\mu_1 = \frac{(\rho_1 - \rho_2)}{(\rho_1 + \rho_2)}$ where ρ_1 is the top or film layer resistivity and ρ_2 is the bottom or substrate resistivity.
- λ : Integration variable
- t: Film thickness

By evaluating the integral in equation 4.11 we get [20]:

$$\frac{\Delta V}{I} = \frac{\rho_{FILM}}{2 \cdot \pi \cdot s} \left[\overbrace{1 + 2 \cdot \sum_{1}^{\infty} \frac{(-\mu_1)^n}{\sqrt{\left[1 + \left(\frac{2 \cdot n}{\tau}\right)^2\right]}}}^{f_0(\tau,\alpha)} \right] \tag{4.12}$$

Where: $\mu_1 = \dfrac{(\rho_1 - \rho_2)}{(\rho_1 + \rho_2)}$ and $\tau = \dfrac{s}{t}$.

By substituting the value of $f_0(\tau,\alpha)$ from equation 4.10 into equation 4.12, the following expression is obtained.

$$\frac{\Delta V}{I} = \frac{\rho_{FILM}}{2 \cdot \pi \cdot s} \left[\overbrace{1 + 4 \cdot \sum_{n=1}^{\infty} \frac{(-\mu_1)^n}{\sqrt{1 + \left(\frac{2 \cdot n}{\tau}\right)^2}} + 2 \cdot \sum_{n=1}^{\infty} \frac{(-\mu_1)^n}{\sqrt{1 + \left(\frac{n}{\tau}\right)^2}}}^{f(\tau,\alpha)} \right] \tag{4.13}$$

$F(\tau,\alpha) = \dfrac{1}{f(\tau,\alpha)}$ was graphed using the result of equation 4.13 and is shown in Figure 4.3:

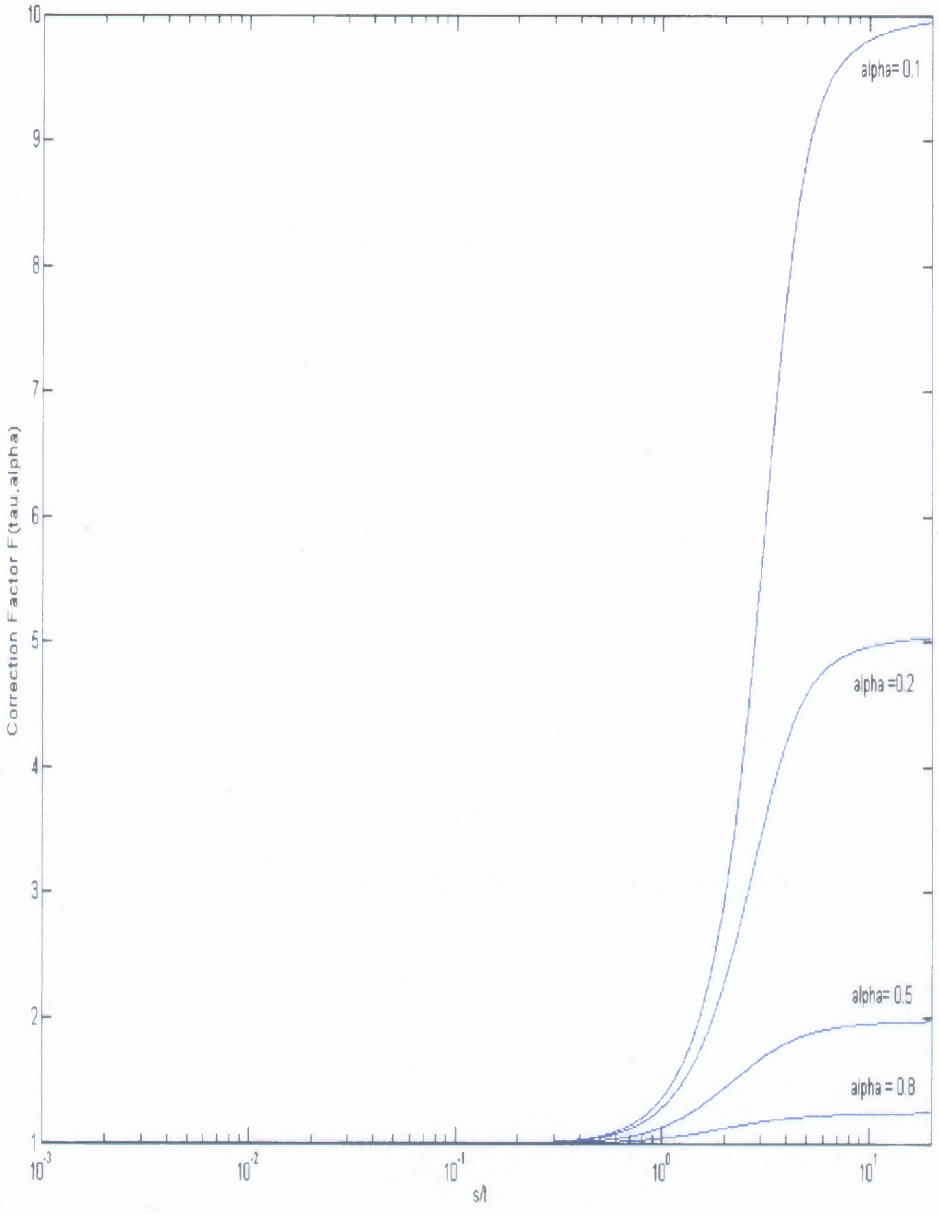

Figure 4.3 Thickness correction factor F (τ,α) versus τ = s/t for two-layer structure Where alpha = =$\rho_{substrate}$ /ρ_{film}.

When alpha ratio is not known, the resistivity of the film and its thickness can be determined

by graphing the curves of $f(\tau,\alpha)$ as a function of s/t for different values of alpha and then matching them to the apparent resistivity curve of $\rho = (2\pi s)*(\Delta V/I)$ measured for different probe spacing.. This method is widely used in geophysics to determine the depth of bedrocks layer under the earth ground. More explanation of this method is provided in Appendix D for consultation.

The resistivity formula used for two-layer structure can be used to approximate surface resistance for certain types of three metal layer case. However, the case of three-layer structure, where the intermediate layer is very thin and highly conductive needs to be analyzed separately using the theory developed for three-layer structure.

The two-point probe method resistance for three-layer structure is expressed as [20]:

$$\frac{\Delta V}{I} = \frac{\rho_1}{2\cdot\pi}\cdot\int_0^{\infty}\frac{1-\mu(\lambda)\cdot e^{-2.\lambda\cdot d_1}}{1+\mu(\lambda)\cdot e^{-2\cdot\lambda\cdot d_1}}\cdot J_0(\lambda\cdot r)d\lambda \tag{4.14}$$

Where

$$\mu(\lambda) = \frac{\rho_1-\rho_2\cdot(1-\mu_2\cdot e^{-2\lambda d_2})/(1+\mu_2\cdot e^{-2\lambda d_2})}{\rho+\rho_2\cdot(1-\mu_2\cdot e^{-2\lambda d_2})/(1+\mu_2\cdot e^{-2\lambda d_2})} \tag{4.15}$$

$\mu_2 = (\rho_2-\rho_3)/(\rho_2+\rho_3)$

$d_1 = Thickness\ of\ upper\ layer$

$d_2 = Thickness\ of$ int $ermidiate\ layer$

$d_3 = Thickness\ of\ the\ bottom\ layer(substrate)$ which considered to be infinite in this model

when the intermediate layer is thin and it's resistivity is low compared to the top and bottom layer resistivity much simpler version of 4.14 can be expressed as [20]:

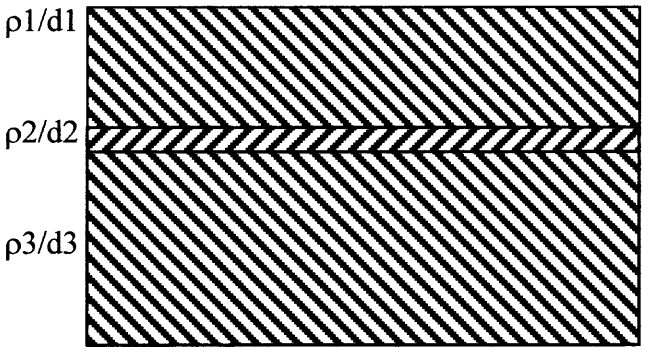

$$\mu = \frac{(\rho_1 - \rho_3 + \lambda \cdot d_2 \cdot \rho_1 \cdot \rho_3 / \rho_2)}{(\rho_1 + \rho_3 - \lambda \cdot d_2 \cdot \rho_{11} \cdot \rho_3 / \rho_2)} \tag{4.16}$$

Letting $d_2 = 0$ for simplicity since the intermediate layer is very thin $\mu(t)$ becomes:

$\mu(\lambda) = \frac{\rho_1 - \rho_3}{\rho_1 + \rho_3}$ which is equal to $\mu_1(\lambda)$ defined for two-point resistivity for two-layer structure in equation 4.12.

As a result, by simple inspection the mutual resistance for this case become similar to the one for two-layer structure, neglecting the effect of the intermediate layer.

In Summary, from the four-point probe theory just reviewed for different structures we can conclude the following statements:

- For bulk material where sample thickness is greater than probe spacing (t>>s), the resistivity is $\rho = (2\pi s)*(\Delta V/I)$. However, for thin layers (t<<s), the resistivity can be computed from $\rho = \pi/ln(2) \cdot t \cdot (\Delta V/I)$.

- For thin film on insulating substrate (t<<s), the resistivity is $\rho = \pi/ln(2) \cdot t \cdot (\Delta V/I)$.

- For film on a "conducting" substrate, the substrate effectively shorts the film when t/s = 0.05 according to Weller. Resistivity measurements are possible theoretically for t/s = 0.2

- For films on high resistivity substrates, the resistivity of the film is $\rho = \pi/ln(2) \cdot t \cdot (\Delta V/I$ *for* (t<<s), neglecting the effect of the substrate.

- For films with resistivity different than the substrate, the correction factor is F (τ,α) in equation 4.1 where $\alpha = \rho_{substrate} / \rho_{film}$ and τ = s/t was presented. Figure 4.3 can be used for determining correction factors for different values of α.

- For the case of three-layer structure where the resistivity of the thin intermediate layer is very low, the model for two-layer structure can be applied to the top and bottom layers, neglecting the effect of the intermediate layer.

4.3 Resistivity Measurement of Ta Films on SiO_2 Substrate

A standard oxidized Si wafer was cut into small samples, about 15 mm by 15 mm. The samples were cleaned by acetone and propanol in an ultrasonic cleaner as described previously in chapter 2. Then, different Ta films (0.02 to 20 μm thickness) were deposited on the SiO_2 samples at different deposition conditions. Deposition conditions of all samples used in this work are listed in Appendix A.

For resistivity measurement, an automatic Resistivity Meter FPP-5000 made by Vecco Company was used to generate most of the data. It is capable of automatic calculation and display of sheet or slice resistivity, V/I, metallization thickness for a given resistivity, and Si P-N type doping. The four-point probe heads used were made from tungsten carbide with a probe spacing of about 1 mm. Figure 4.4 shows the resistivity meter used at NJIT's clean room.

Figure 4.4 Picture of resistivity meter.

During resistivity measurement, the four probes were placed approximately at the center of our samples in order to minimize the edge effect since our sample lateral area are very small

compared to standard wafer area. Resistivity values for all different films were measured based on their film thickness determined by a stylus Profilometer, Sloan Dektak II. To investigate the film phases, X-ray analysis of the films was done using Philips Expert MPD instrument with Cu Kα radiation. The ratio of XRD relative peak intensity α-Ta (110) to β-Ta (002) were tabulated in Appendix A. To analyze the relation between the resistivity and phase composition of the deposited films, resistivity values, relative α-phase peak intensity and film thickness were analyzed and are presented in Table 4.1 to 4.3. The relative α-phase peak intensity was defined as:

$$R_\alpha \cong \frac{I_\alpha(110)}{I_\alpha(110)+I_\beta(002)}$$

Where:

$I_\alpha(110)$: alpha peak intensity at (100) orientation.

$I_\beta(002)$: beta peak intensity at (002) orientation.

The data was sorted into three phase composition groups: Alpha phase ($R\alpha>0.1$), mixed phases, and beta phase ($R\alpha>0.1$) according to XRD results.

Table 4.1 Resistivity Values for Alpha Tantalum Phase on SiO_2 Substrates

Film Thickness [μΩ]	Film Resistivity [μΩ. cm]	Rα
20.21	13.2	1
11.01	14.5	1
3.23	14.7	1
3.01	15	1
4.30	15.5	1
11.45	16	1
1.53	16.24	1
5.84	19	1
1.70	21	1
2.17	22	1
1.89	23	1
8.82	42	1

Table 4.2 Resistivity Values for Mixed Tantalum Phase on SiO_2 Substrates

Film Thickness [μΩ]	Film Resistivity [μΩ. cm]	Rα
3.07	18	0.903
1.52	19	0.989
1.63	20.2	0.910
1.60	32	0.086
2.33	34	0.848
1.43	73.8	0.064
1.58	80	0.358
1.35	150	0.019
2.76	150	0.016
2.44	150	0.001
.29	154.2	0.052
12.11	160	0.017
11.87	188	0.019
1.50	190	0.096
2.10	236	0.006
.97	240	0.013

Table 4.3 Resistivity Values for Beta Tantalum Phase on SiO_2 Substrates

Film Thickness [μΩ]	Film Resistivity μΩ. cm]	Rα
7.54	87	0
1.89	153	0
1.87	157	0

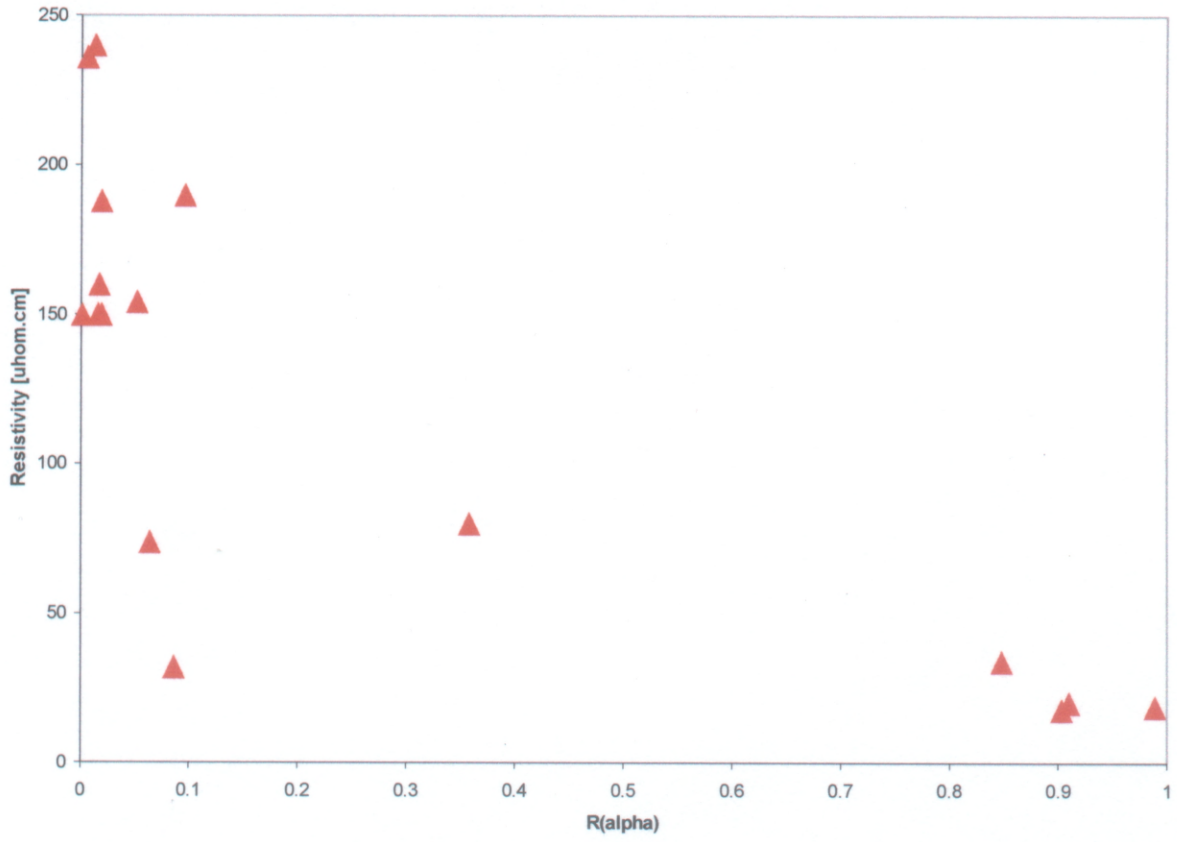

Figure 4.5 Resistivity as a function of Rα for silicon oxide substrates from Table 4.2.

From Table 4.1 the resistivity of alpha tantalum ranges from 13.2 to 42 μΩ.cm. From Table: 4.3 beta tantalum resistivity varies from 87 to 157 μΩ.cm. The resistivity range obtained for mixed tantalum phases varies from 18 to 240 μΩ.cm, Table:4.2.To get a better understanding of how the phase composition of tantalum films effects resistivity values, the resistivity of tantalum films was plotted as a function of relative alpha phase intensity Rα (Figure: 4.5).

The graph shows that the resistivity decreases with the increase of the relative intensity of alpha phase Rα. However, samples with 32 and 73 μΩ.cm resistivity do not follow the resistivity behavior just described.

4.4 Resistivity Measurement of Ta Films on Si Substrate

A standard (100) Si wafer with a resistivity of 15-20 Ω.cm was cut into small square samples, about 15 mm by 15 mm. The samples were cleaned by acetone and propanol in an ultrasonic cleaner as described previously in chapter 2. Then different Ta films (.78 to 11 μm thickness) were deposited on Si samples at different deposition conditions. Deposition history of all samples used in this work are listed in Appendix A. Both resistivity measurement and XRD analysis were performed as described in section 4.12. The results are shown in Table 4.4 to 4.6.

Table 4.4 Resistivity for Alpha Tantalum Phase on Si Substrates

Film Thickness [μΩ]	Film Resistivity [μΩ.cm]	Rα
4.11	13.5	1
8.97	13.94	1
2.81	15.5	1
2.78	16	1
2.78	16.5	1
26.3	16.85	1
4.10	18.4	1
7.44	18.5	1
1.72	19	1
2.31	20	1
1.77	22.7	1
.78	23	1
.11	201	1

Table 4.5 Resistivity for Mixed Tantalum Phase on Si Substrates

Film Thickness [μΩ]	Film Resistivity [μΩ.cm]	Rα
2.95	16	0.957
1.79	20.1	0.775
1.94	26	0.975
11.62	60.5	0.445
4.78	65	0.104
1.54	124	0.018
1.65	188	0.0008

The resistivity of alpha tantalum ranges from 13.5 to 23 μΩ. cm, Table 4.4. Mixture of both phases ranges from 16 to 188 μΩ.cm, Table 4.5. To get a better understanding of how the phase composition of tantalum films affects its resistivity, resistivity values, relative α-phase peak intensity (defined in section 4.1.2) and film thickness are presented in Figure 4.5.

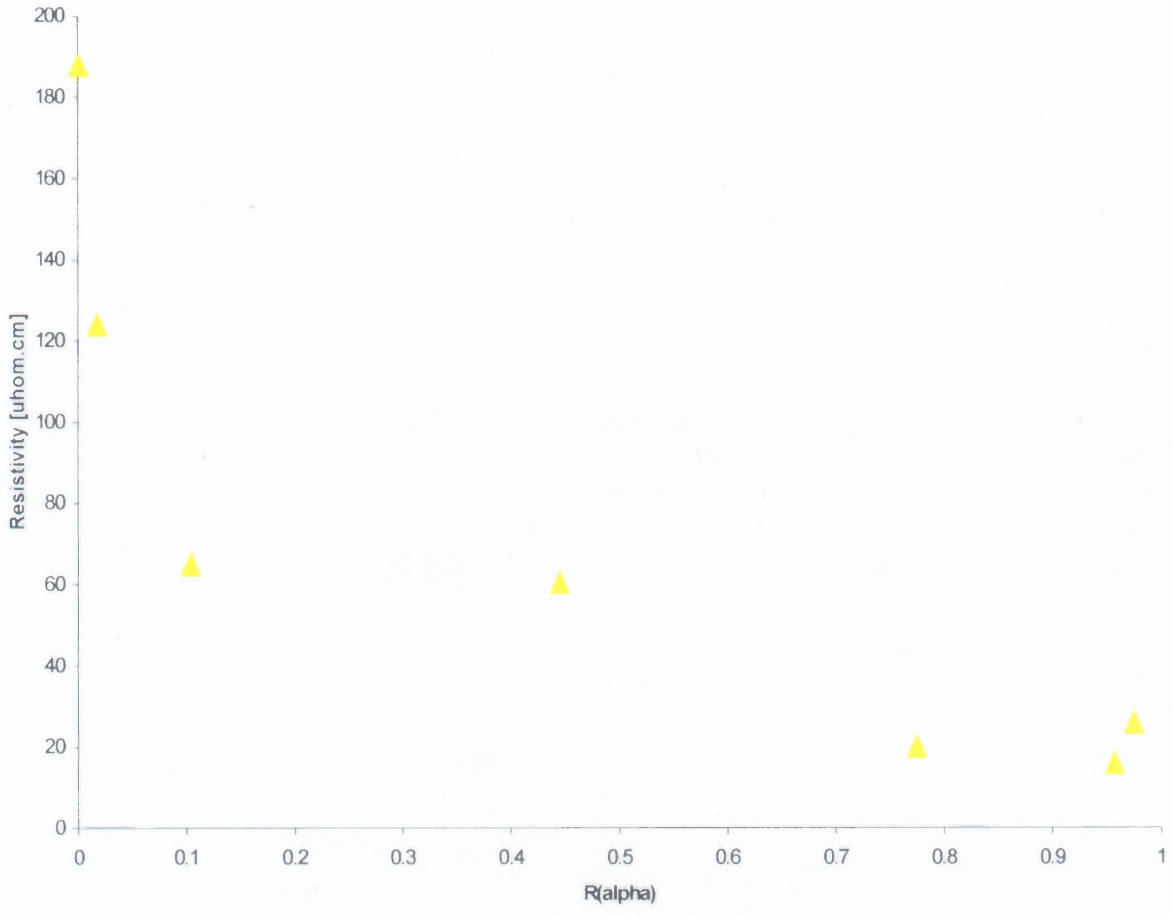

Figure 4.6 Resistivity as a function of Rα for silicon substrates from Table 4.4.

The resistivity of tantalum films on silicon substrates in Figure 4.6 seems to decrease with the increase of the relative alpha peak intensity Rα, almost the same behavior as for films on silicon oxide bottom in Figure 4.5 except the sample with 60.5 μΩ. cm.

In Summary, Resistivity behavior for both Si and SiO_2 substrates are concluded to be the same .The samples can divided into three groups:

- Samples with mostly beta phase composition ($R\alpha<0.1$) with the exception of two samples.
- Samples with mixture of both alpha and beta phases.
- Samples with mostly alpha phase composition.($R\alpha>0.1$)

The resistivity of tantalum film decrease with the increase of the relative alpha peak intensity.

The four-point probe method measures the average resistivity in the case of mixed phase tantalum films. Therefore, the resistivity measurement results depends on the way both alpha and beta phase are distributed in the film. Assuming a mostly beta film with some islands of alpha phase in it distributed randomly. If the current line created by the injected current establishes a easy path through the alpha islands, the voltage drop measured at the surface of the film is influenced, resulting in a resistivity value different that one expected for beta. However, films that are mostly alpha with some beta islands distributed randomly in them might not be effected by the existing alpha tantalum. From theses two example, we deduce that the resistivity measurement for mixed phase sometimes can fail.

XRD-analysis used on our samples have the capability of analyzing about a micron near the film top surface. And that is due to the nature of the x-ray beams used.Therefore, any change of the material phase at the bottom of the film can not be detected and this can justify the sample with 73 $\mu\Omega$.cm with has an $R\alpha$ of 0.06.

Both XRD-analysis and resistivity measurement are recommended to be used in order to get a full understanding of the film structure.

4.5 Resistivity Measurement of Ta Films on Steel Substrate

To verify the theory for different conducting substrates, covered previously in section 5.2, two different samples were requested from Benet Laboratory at Watervliet Arsenal. Sample #1 consists of 145 μm Ta (Pure Alpha Phase) / 5 μm Nb / Thick curved gun steel substrate. The 5 μm Nb film was used as a buffer layer to promote alpha phase tantalum. Sample #2 consists of 120 μm (Pure Beta Phase) / Thick curved gun steel substrate. These samples were sectioned from a 45 mm gun steel tubes.

In order to reach less than 0.5 mm probe spacing, which is uncommon and costly in today's market, a micromanipulator station was used along with an hp 4551-Semiconductor Parameter Analyzer for our resistivity measurements. The micromanipulator consists of four tungsten carbide sharp long needls that can be positioned manually under an optical microscope. Two of the needles are used for current injection and collection, the remaining probes are used to detect the voltage drop. The four probes were set up in in-line configuration as shown in Fig: 4.1. The hp analyzer was configured both to generate a 100 mA and to measure the voltage drop.

Resistivity measurements were done on sample #1 and sample #2 with different probe spacing ranging from 4 mm down to 0.25 mm. ($\Delta V/I$) as function of probe spacing for both samples is plotted in Fig: 4.7. For probe spacing greater than 1 mm spacing, the ($\Delta V/I$) for both sample is the same. Once the spacing gets smaller that 1mm, differences in ($\Delta V/I$) values for both samples are noticed. Meaning that the steel substrate shorting effect is diminishes when the spacing is very small that 1 mm spacing.

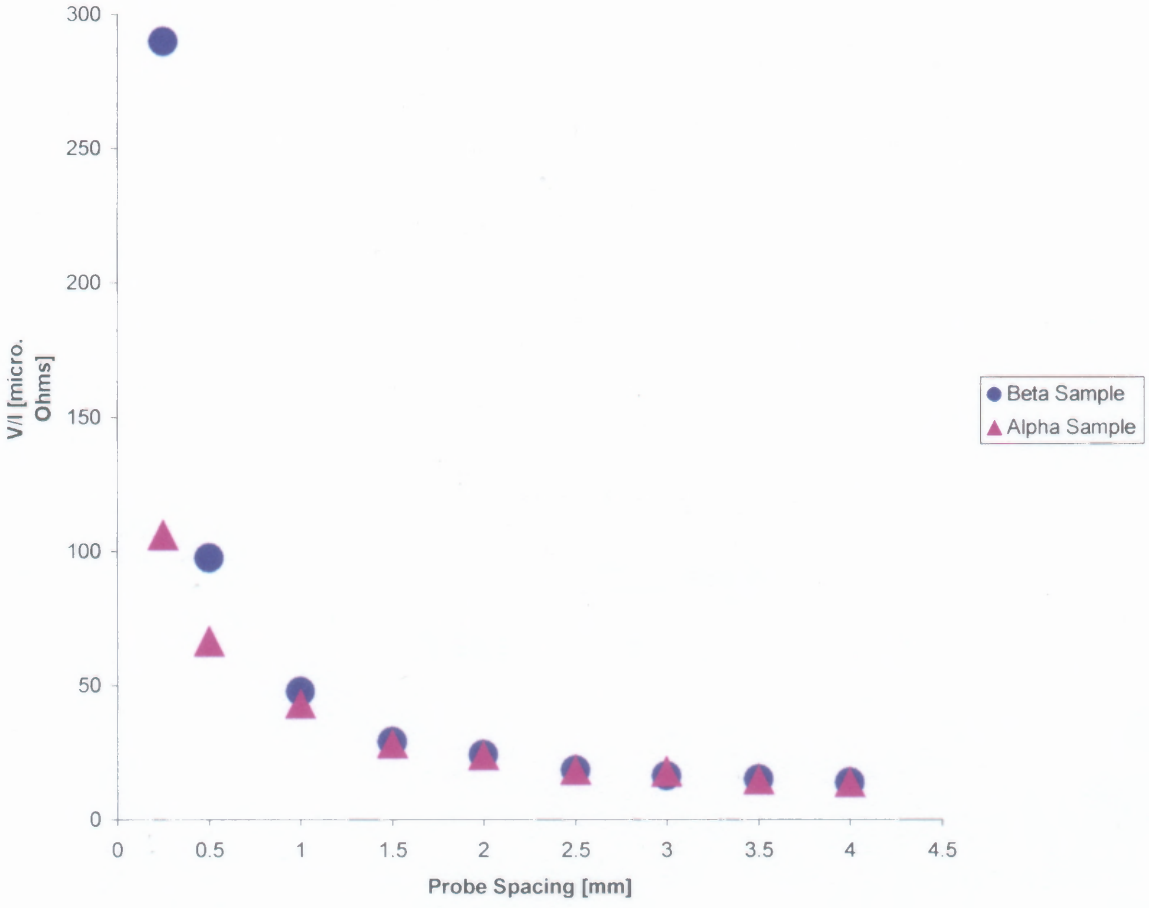

Figure 4.7 V/I as function of Probe Spacing (I=100Ma).

Using Equation 4.1 combined with the thickness correction factor shown in Fig 4.3, the resistivity of both samples was calculated and is shown in Figure 4.8. For the beta sample, the curve for $\alpha = \rho_{substrate} / \rho_{film} = 0.1$ was used to generate the correction factor for the values of s/t that are less than 1 [mm]. For the alpha sample the correction factor for $\alpha = \rho_{substrate} / \rho_{film} = 1$ is unity according to equation 4.13. The values of resistivity for probe spacing greater than 0.5 mm were not computed because they reflect the resistivity of the substrate.

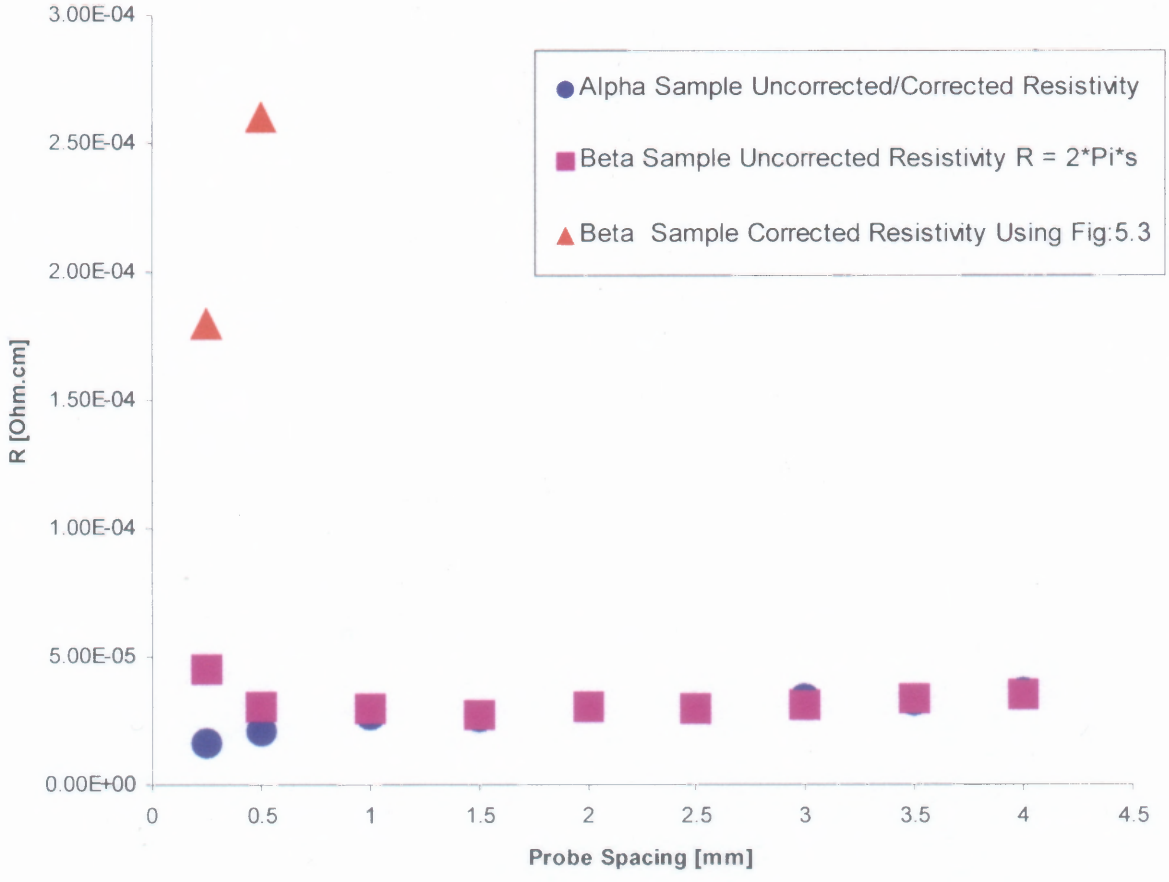

Figure 4.8 Resistivity as function of Probe Spacing (I=100Ma).

The average resistivity for the beta sample is around 220 μΩ. cm. For alpha sample the average resistivity is around 18.75 μΩ. Cm, which is in agreement with values reported in the literature[2].

Weller stated that when the film is thick the resistivity of the conducting substrate becomes irrelevant because the current flows near the surface of the thick film without reaching the substrate. In order to verify Weller's statement, resistivity measurement of a thick bulk tantalum film (≈ 0.8 mm) fussed on thick steel was done for different probe spacing and the results are shown in Fig 4.9.

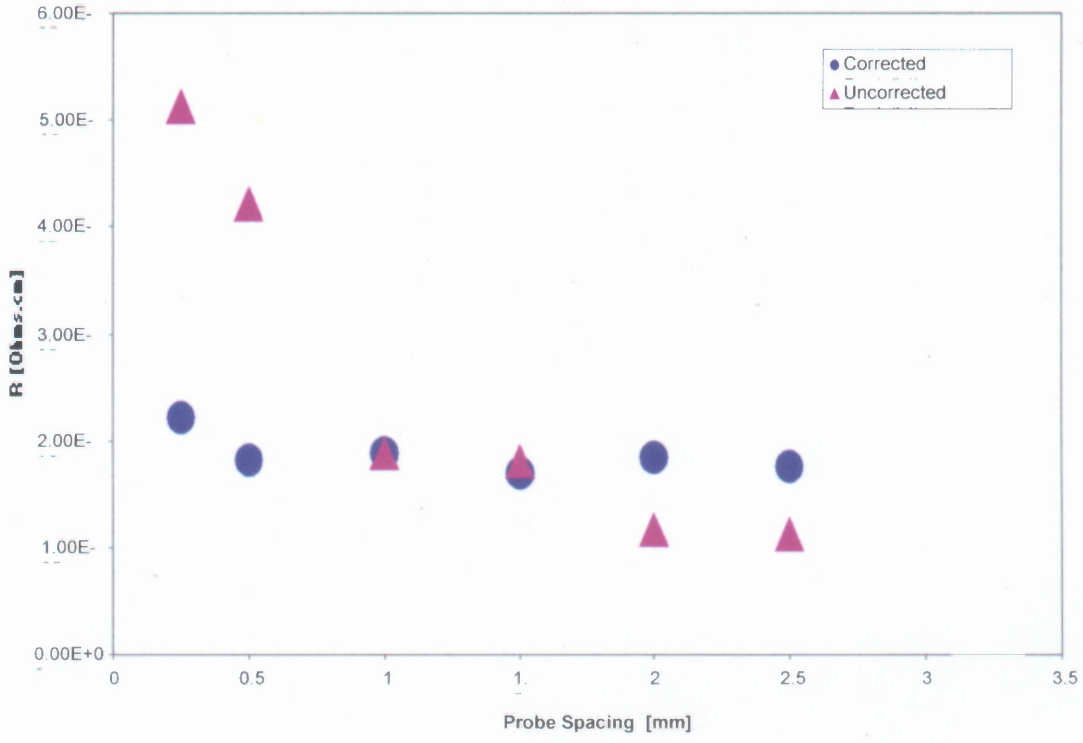

Figure 4.9 Corrected and Uncorrected Resistivity for Thick Ta film in Function of Probe Spacing.

The resistivity of the thick film was computed using equation 4.7 for the case of a conducting boundary (neglecting the substrate effect since the film is thick). The average resistivity of the thick film is 18.21 μΩ. cm which agrees well with alpha tantalum.

CHAPTER 5

SUMMARY

Resistivity measurements of tantalum coatings (1-20 μm) on silicon and silicon dioxide substrates were made using the four-point probe method and correlated with the phase composition of the films obtained by XRD. The resistivity method was effective in distinguishing between α-Ta and β-Ta structures on Si and SiO_2 substrates. Alpha phase resistivity ranged from 13.5 to 42 μΩ.cm and beta phase from 87 to 157 μΩ.cm. These resistivity results were consistent with the values found in literature [1]. For coatings with mixed phases, the four-point probe method resulted in an average resistivity, which depends not only on the relative phase composition but also on the distribution of α and β grains in the film. This may explain discrepancies, found on the two samples, between the XRD and the resistivity measurements results.

Four-point probe resistivity measurements on tantalum deposited on steel are influenced by the low resistivity of the substrate, which effectively shorts the current if the probe spacing is comparable to the coating thickness. To study this effect, four-point probe measurements of thick coatings, up to 0.8 mm, were made with varying probe spacing from 0.25 to 4 mm. From the analysis of these experiments it was concluded that to distinguish between alpha and beta phase resistivities, the probe spacing to film thickness ratio of at least 0.2 is required. This is in agreement Weller's theoretical study [14]. The method of Sunde [20] can be applied to obtain corrections to the resistivity of coatings measured on substrates with known resistivity and a given spacing to thickeness ratio.

Recent advances in micro-fabrication technology made it possible for companies like Copenhagen Applied Research to fabricate microscopic four-point probe. These probes are three orders of magnitude smaller than the conventional ones made commercially. Spacing of these probes, as small as 500 nm was reported recently [22]. This will allow measuring the resistivity of films as thin as 2.5 μm conducting substrates. Figure 4.10 shows an SEM picture of the fabricated microscopic-probes.

Ta coatings investigated in this work were deposited by DC magnetron sputtering. The surface of steel substrates was prepared using different methods, which included grinding, polishing, electrochemical cleaning and in-situ sputter etching. The substrate surface morphology and roughness was measured with atomic force microscopy (AFM). The smoothes steel surface was obtained by polishing with a suspension of 50 nm silica particles, which resulted in the surface roughness as low as 5.1 nm was measured on 30 μm x 30 μm scan area. Sputter etching in Ar gas resulted in the formation of characteristic cones on steel surface. No influence of various surface preparation methods on the phase of Ta was observed. However, cleaning, especially sputter-etching, was found to enhance film adhesion.

CONCLUSION

- It has been demonstrated that the phase composition of tantalum films and coating can be evaluated by the four-point probe resistivity measurements.Thin films deposited on highly resistive and insulating substrates, such as silicon and silicon dioxide, can be evaluated by standard probes with spacing of approximately 1 mm. The resistivity of coatings on highly conductive steel substrates, however, can be measured only when their thickness is approximately five times greater than the probe spacing. Microprobes with the spacing as small as 500 nm, which currently are being developed, are suggested for future measurements of films with thickness down to 2.5 μm.
- No influence of various steel surface preparation method, including, polishing, electrochemical cleaning and in-situ sputter etchings, on the phase of Ta was observed. However, cleaning, especially sputter-etching, was found to enhance film adhesion.

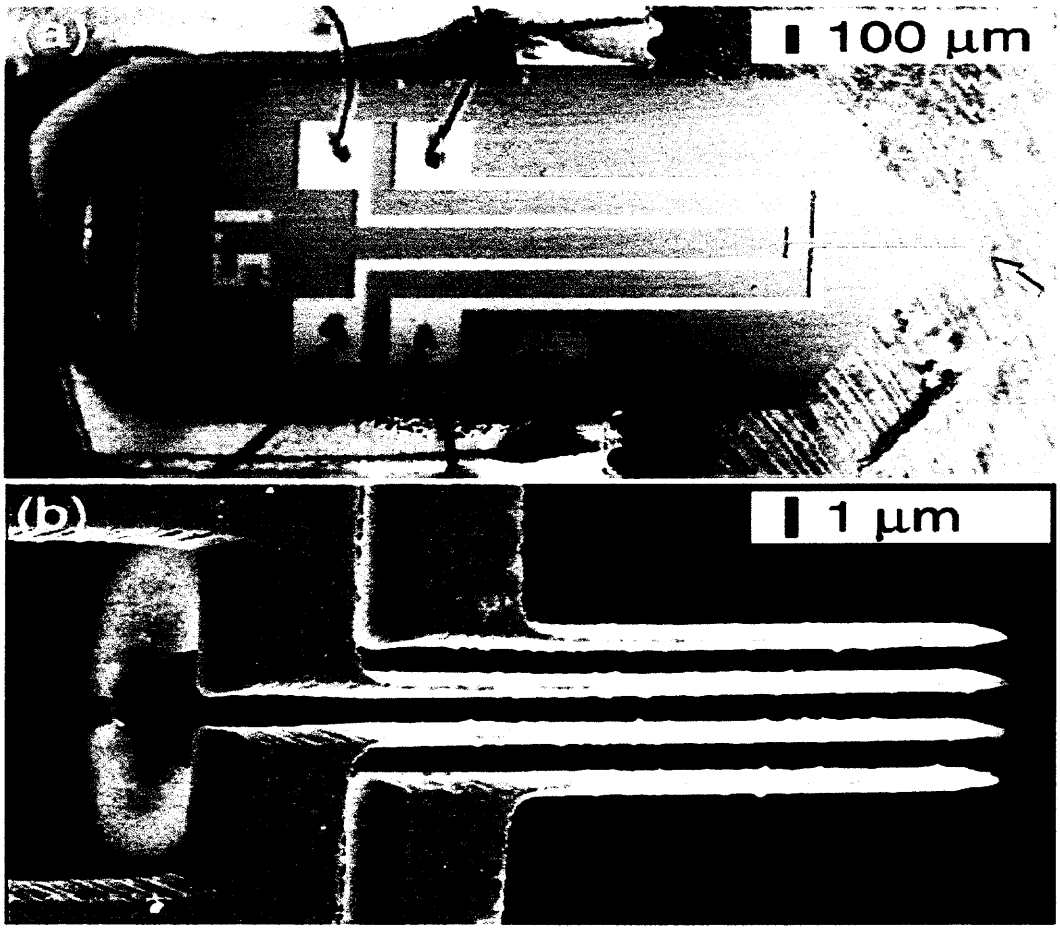

Figure 4.10 (a) Scanning electron micrograph of the four-point probe chip (b) Close up of the resistivity electrodes.

APPENDIX A

GRAPH OF STEEL DEPTH IN FUNCTION OF PARTICLE SIZE GRINDING

The graph below shows the change in steel surface depth caused by different particle sizes.

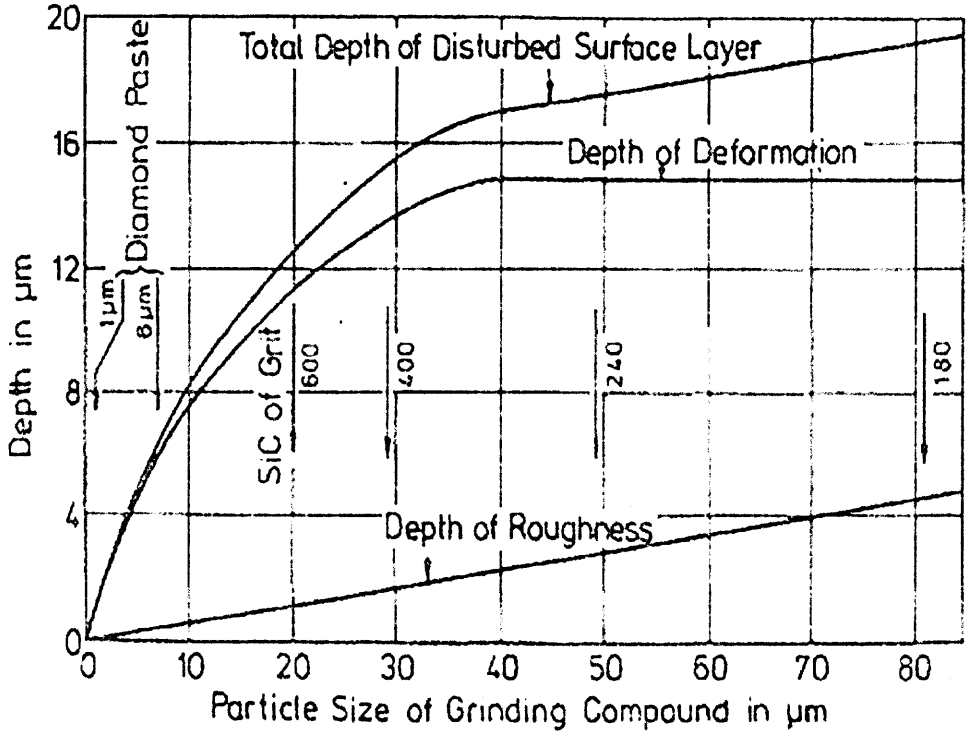

APPENDIX B

DEPOSITION CONDITIONS OF SAMPLES RELATED TO THIS WORK

The table below is a description of depositon conditions of Ta films on different substrates.

Date	Pressure [mTor]	Flow Gas [sccm]	Voltage	Current	Power	Time	Film Thickness [A]	Temp [C]	R[um.cm]	Alpha(110) /Beta(002)
Pta01c/070901	20	Ar/18	300	0.5	150	15	12246	350	181.8	0.05:100
Pta02c/070901	22	Ar/18	300	0.5	150	15	14341	386	73.8	6.9:100
Pta01c/071301	23	Ar/18	300	1	300	1.22	2852	25	154.2	5.54:100
Pta02c/071301	23	Ar/18	300	1	300	10	18150	260	92.1	0.15:100
Pta03c/071301	20	Ar/18	300	0.5	150	20.3	15308	309	16.24	Alpha
Pta01c/071901	23	Ar/18	300	1	300	10	16335	258	20.2	100:9.88
Pta02c/071901	23	Ar/18	300	1	300	10	15826	315	80	55.8:100
Pta01c/072701	23.1	Ar/18	300	1	300	10	18812	188	153	Beta
Pta02c/072701	23.3	Ar/18	300	1	300	10	16014	233	32	9.47:100
PTa02c/082401	1	Ar/1.5	450	0.25	112.5	120	75380	70	87	0.06:100
PTa03c/082401	1	Ar/1	450	0.3	135	30	15211	200	19	100:1.05
PTa04c/082401	1	Ar/1	450	0.3	135	30	21705	250	22	Alpha
PTa05c/082401	1	Ar/1	450	0.3	135	30	17008	300	21	100:0.13
PTa06c/082401	1	Ar/1	450	0.3	135	30	18836	350	23	Alpha
PTa07c/082401	1	Ar/1	550	0.3	165	10.3	6672	350	21	Alpha
PTa02o/082401	1	Ar/1.5	450	0.25	112.5	120	47876	70	65	11.5:100
PTa03o/082401	1	Ar/1	450	0.3	135	30	19439	200	26	100:2.15
PTa04o/082401	1	Ar/1	450	0.3	135	30	17213	250	19	Alpha
PTa05o/082401	1	Ar/1	450	0.3	135	30	22254	300	20	Alpha
PTa06o/082401	1	Ar/1	450	0.3	135	30	23106	350	20	Alpha
PTa07o/082401	1	Ar/1	450	0.3	165	10.3	7836	350	23	Alpha
Pta01c/100301	5	Ar/2.8	300	0.5	150	60	54999	300	16.3	Alpha
Pta02c/100301	5	Ar/2.8	300	0.5	150	30	31050	300	17.5	N/A
Pta03c/100301	5	Ar/2.8	250	0.2	50	60	18735	70	157	Beta
Pta05c/100301	5	Ar/2.8	250	0.2	50	60	14951	70	190	10.7:100
Pta06c/100301	5	Ar/2.8	300	0.5	150	30	23314	300	34	100:17.8
Pta06o/100301	5	Ar/2.8	250	0.2	50	60	13750	70	154.9	N/A

PTa01c/081001	10.8	Ar/2	300	0.4	120	30	24499	70	150	0.13:100
PTa02c/081001	5	Ar/2	300	0.4	120	30	27620	70	150	1.63:100
PTa03c/081001	1	Ar/2	300	0.4	120	30	27410	70	22	100:4.86
PTa04c/081001	1	Ar/2	300	0.4	120	0.25	244	70	94.3	100:7.71
PTa05c/081001	1	Kr/1.5	350	0.4	140	15	13505	70	150	2:100
PTa06c/081001	1	Kr/1.5	360	0.4	144	15	13626	70	150	Beta
PTa07c/081001	1	Kr/1.5	400	0.4	160	15	9656	70	240	1.3:100
PTa01o/081001	10.8	Ar/2	300	0.4	120	30	15480	70	124	1.8:100
PTa02o/081001	5	Ar/2	300	0.4	120	30	17832	70	20.1	92.1:26.7
PTa03o/081001	1	Ar/2	300	0.4	120	30	17644	70	22.7	8.14:00
PTa04o/081001	1	Ar/2	300	0.4	120	0.25	bad step	70	N/a	0.01:00
PTa05o/081001	1	Kr/1.5	350	0.4	140	15	16592	70	188	0.08:100
PTa06o/081001	1	Kr/1.5	360	0.4	144	15	10087	70	122.3	0:0
PTa07o/081001	1	Kr/1.5	400	0.4	160	15	11185	70	201	4.13:00

PTa01c/083001	1	Ar/1	470	0.4	188	60	62005	300	23	Alpha
PTa02c/083001	1	Ar/1	450	0.4	180	90	58497	300	19	Alpha
PTa03c/083001	1.1	Kr/1.1	550	0.3	165	65	43008	250	15.5	Alpha
PTa04c/083001	2.5	Kr/2.5	550	0.4	220	90	88267	250	42	Alpha
PTa01o/083001	1	Ar/1	470	0.4	188	60	41098	300	18.4	2.57:00
PTa02o/083001	1	Ar/1	450	0.4	180	90	74357	300	18.5	34.26:00
PTa03o/083001	1.1	Kr/1.1	550	0.3	165	6590	41134	250	13.5	69.2:0.76
PTa04o/083001	2.5	Kr/1.1	470	0.4	220		89721	250	13.94	100:00

PTa01c/092501	5	Ar/2.9	300	0.4	120	230	110151	300	14.5	Alpha
PTa02c/092501	5	Ar/2.9	300	0.4	150	300	202151	300	13.2	Alpha
PTa01o/092501	5	Ar/2.9	300	0.4	150	300	262906	300	16.85	Alpha

PTa01c/081601	1.1	Kr/1.5	400	0.4	160	120	121129	70	160	1.69:97.3
PTa02c/081601	1.1	Kr/1.5	390	0.4	156	30	30726	200	18	100:10.7
PTa03c/081601	1.1	Kr/1.5	380	0.4	152	30	30199	250	15	Alpha
PTa04c/081601	1.1	Kr/1.5	175	0.4	150	30	32156	300	15	74.22:00
PTa05c/081601	1.1	Kr/1.5	360	0.4	144	30	32331	350	14.7	Alpha
PTa06c/081601	1.1	Kr/1.5	250	0.4	140	120	114516	350	16	Alpha
PTa01o/081601	1.1	Kr/1.5	400	0.4	160	120	116165	70	16	80.1:100
PTa02o/081601	1.1	Kr/1.5	390	0.4	156	30	29563	200	15.5	100:4.48
PTa03o/081601	1.1	Kr/1.5	380	0.4	152	30	27642	250	16.5	Alpha
PTa04o/081601	1.1	Kr/1.5	375	0.4	150	30	28109	300	15.6	Alpha
PTa05o/081601	11	Kr/1.5	360	0.4	144	30	27851	350	18.3	Alpha
PTa06o/081601	1.1	Kr/1.5	350	0.4	140	120	9513	350	16.2	100:1.38

PTa05c/081001	1	Kr/1.5	350	0.4	140	15	13505	70	148	2:100
PTa06c/081001	1	Kr/1.5	360	0.4	144	15	13626	70	158	Beta
PTa07c/081001	1	Kr/1.5	400	0.4	160	15	9656	70	264	1.3:100
PTa03c/083001	1.1	Kr/1.5	550	0.3	135	65	43008	250	15.5	65.38
PTa04c/083001	2.5	Kr/1.5	550	0.4	220	90	88267	250	42	Alpha

The symbols in the sample condition table stand for:

- PTa xx : sample holder number
- C: Silicon substrate was used
- O: Silicon oxide was used
- /XXXXXX: Date when the sample was deposited.

APPENDIX C

X-RAY DIFFRACTION LINES FOR ALPHA AND BETA TANTALUM FILMS MEASURED ON SOME SAMPLES

The graphs shows XRD peaks measured for two Ta films tantalum grown on steel.

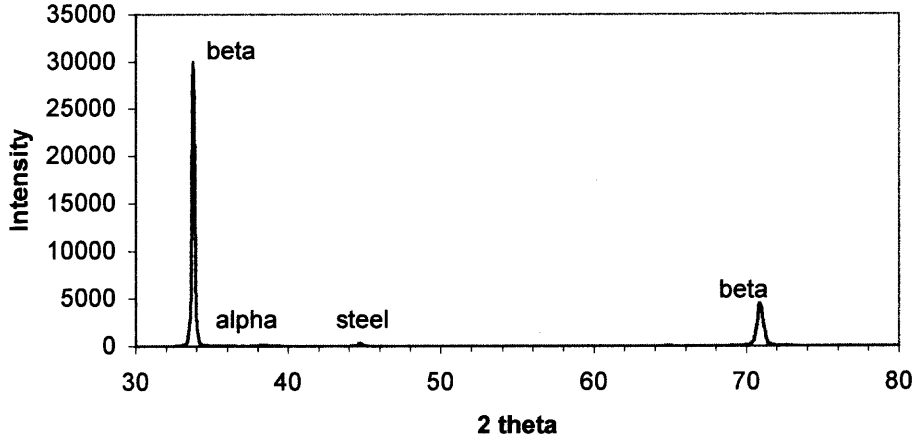

X-ray analysis of tantalum films showing peaks for alpha and beta tantalum deposited on steel for two different samples.

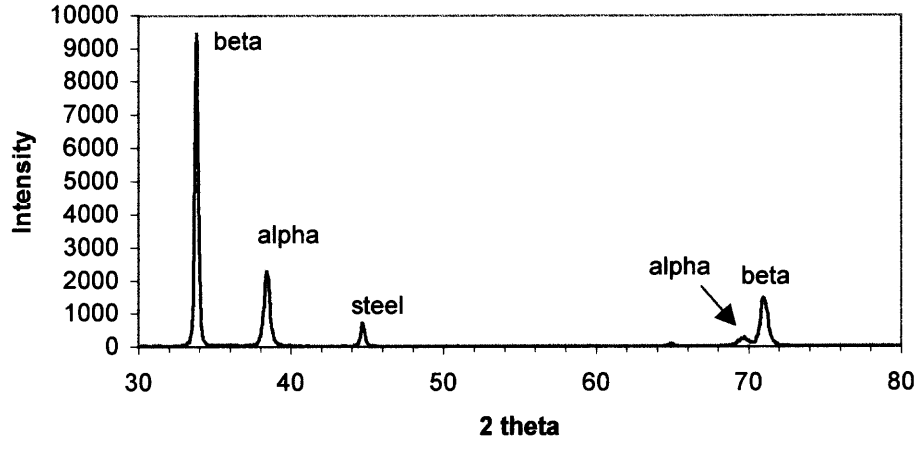

APPENDIX D

EXPLANATION OF CURVE FITTING METHOD

The apparent resistivity presented in section 4.14 for beta tantalum film on steel substrate sample can be corrected given the ratio of substrate resistivity to film resistivity. For most of the tantalum films sputtered on steel substrate, the only known parameters are the film thickness and the substrate resistivity. The suggested solution for this problem is to find the film resistivity by matching its apparent resistivity curve as a function of s to a set of theoretical apparent resistivity curves function of s/t. A set of such function is shown below:

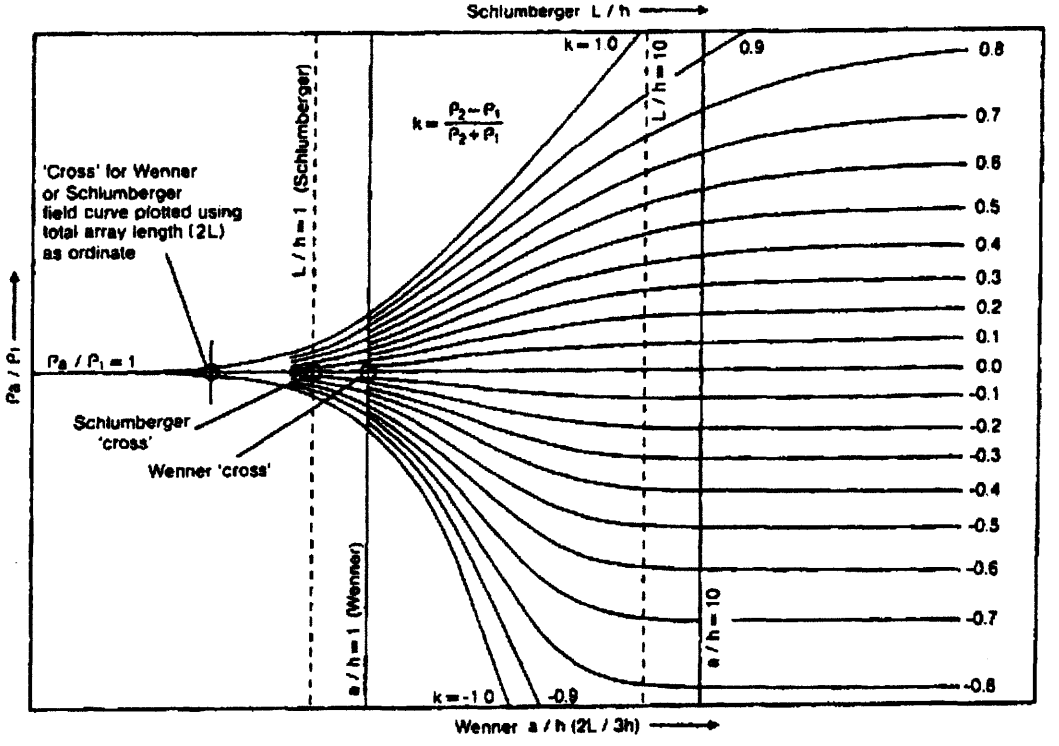

Master curves developed for a two-layer structure.

These curves are known in geophysics as master curves. They represent the theoretical change of apparent resistivity to top layer resistivity ratio as a function of s/t. The curve fitting can be accomplished either manually or by using computer interpretation tools. An example of the curve fitting procedure is described in [21].

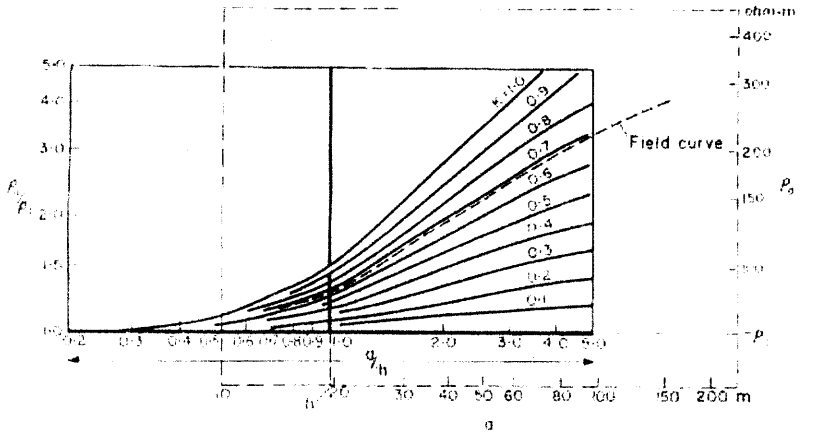

The curve fitting consists of the following steps:

- Plot smoothed field data on log-log graph transparency.
- Overlay transparency on master curves keeping axes parallel.
- Note electrode spacing on transparency at which (a / h=1) to get interface depth.
- Note electrode spacing on transparency at which (r_a / r_1 =1) to get resistivity of layer 1.
- Read off value of k to calculate resistivity of layer 2 from:

Where

- R1: Top layer resistivity
- Ra: Apparent resistivity
- A: Electrode spacing
- H: The depth of the top layer

REFERENCES

1. S.L Lee, D. Windover, "Phase, residual stress, and texture in triode-sputtered tantalum coatings on steel", Surface and Coatings Technology, vol. 108-109, pp. 65-72, 1998.

2. Wen Luh Yang, Wen-Fa Wu, Don-Gey Liu, Chi-Chang Wu, Keng Liang Ou, "Barrier capability of TaNx films deposited by different nitrogen flow rate against Cu diffusion in Cu/TaNx/n+ -p junction diodes", Solid-State Electronics, vol. 45, pp. 149-158, 2001.

3. Hiroyuki Shimada, Ichiro Ohshima, Takeo Ushiki, "Tantalum Nitride Metal Gate FD-SOI CMOS FETs Using Low Resistivity Self-Grown bcc-Tantalum Layer", IEEE Transactions On Electron Devices, vol. 48, no. 8, 2001.

4. W M Pasadowski, "Sustained self sputtering of different materials using dc magnetron", Vacuum, vol. 46, no. 8-10, pp. 1017-1020, 1995.

5. D.W. Matson, M.D. Merz, and E.D. McClanahan, "High rate sputter deposition of wear resistant tantalum coatings", J. Vac. Sci. Techno, vol. 10, no. 4, pp. 1791-1796,1992

6. Wolf and R. N. Tauber, Silicon Processing for the VLSI Era Vol.1- Process Technology, Lattice Press, Sunset Beach, CA, 2000.

7. Webelement URL http://advanced-energy.com/Upload/white5.pdf (2000)

8. Bhavin Shah, "DEPOSITION OF TANTALUM ON STEEL BY SPUTTERING", Master's Thesis, January 20001, Material Science and Engineering. New Jersey Institute of Technology, Newark.

9. Andreas W. Momber, Yat C. Wong, Edwin Budidharma, Riny Tjo, "Surface profiling of low-carbon steel with supersonic waterjets", Wear, vol. 249, pp. 853-859, 2001.

10. Kari Koski, Jorma Holsa, Jacques Ernoult, Andre Rouzaud, "The connection between cleaning and adhesion of thin solid films", Surface and Coatings Technology, vol. 80, pp. 195-199, 1996.

11. Gunter Petzow and Veronica Carle, Metallographic Etching, ASM International Materials Park, OH 44073-0002.

12. H.Ollendorf, D.Schneider, "Comparative Study of Adhesion Test Methods for Hard Coatings", Surface and Coatings Technology, Vol 113, pp. 86-102, 1999.

13. J L Vossen, "The preparation of substrates for film deposition using glow discharge techniques", J. Phys. E. Sci. Instrum, vol. 12, p. 159,1979.

14. Weller, Robert A., "An algorithm for computing linear *four-point probe* thickness correction factors.", Rev. Sci. Instrum., vol. 72, pp. 3580-3585, 2001.

15. Webelement URL http://four-point-probes.com/fpp.html 2001

16. L. B Valdes, "Resistivity Measurements on Germanium for Transistors", Proc. I.R.E., pp. 420-427, February, 1954.

17. J. Albers and H. L. Berkowitz, "The Relation Between Tow-Probe and Four-Probe Resistances on Nonuniform Structures", J. Electrochem. Soc, vol. 131, pp. 392-398, October, 1984.

18. J. Albers and H. L. Berkowitz, "An Alternative Approach to the Calculation of Four-Probe Resistances on Nonuniform Structures", J. Electrochem. Soc, vol. 13, no.10, pp. 2453-2456, October, 1985.

19. J.J. Kopanski, John Albers, G..P. Carver, and J. R. Ehrstein, "Verification of the Relation Between Tow-Probe and Four-Probe Resistances as Measured on Sillicon Wafers", J. Electrochem, vol. 137, no.12, December 1990.

20. Erling D. Sunde, "Earth Conduction In Effect In Transmission Systems", Dover Publications, Inc, New York.

21. D H. Griffiths, "Applied Geophysics For Geologists And Engineers".

22. C.L. Peter, T.M. Hansen, P. Boggild, A. Boisen, O. Hansen, T. Hassenkam, F.Grey, "Scanning microdcopic four-point conductivity probes", Sensors and Actuaturs, vol. 96, pp. 53-58, 2002.